Differentiation of an upper crustal magma reservoir via crystal- melt separation recorded in the San Gabriel pluton, central Chile

Research Paper

THEMED ISSUE: Different Personalities of Granites and Rhyolites: Silicic Magmas from the Lower Crust to the Surface

GEOSPHERE

GEOSPHERE, v. 19, no. 2

https://doi.org/10.1130/GES02535.1

12 figures; 1 set of supplemental files

CORRESPONDENCE: italo.payacan@umayor.cl

CITATION: Payacán, I., Gutiérrez, F., Bachmann, O., and Parada, M.Á., 2023, Differentiation of an upper crustal magma reservoir via crystal-melt separation recorded in the San Gabriel pluton (central Chile): Geosphere, v. 19, no. 2, p. 348–369, https://doi.org/10.1130/GES02535.1.

Science Editor: Shanaka de Silva
Guest Associate Editor: Ayla Pamukcu

Received 21 March 2022
Revision received 31 October 2022
Accepted 6 December 2022

Published online 23 February 2023

Differentiation of an upper crustal magma reservoir via crystal-melt separation recorded in the San Gabriel pluton, central Chile

I. Payacán[1,2,3], F. Gutiérrez[4], O. Bachmann[5], and M.Á. Parada[1,6]

[1]Departamento de Geología, Universidad de Chile, Plaza Ercilla 803, Santiago 8370450, Chile
[2]Escuela de Geología, Universidad Mayor, Manuel Montt 367, Providencia, Santiago 7500994, Chile
[3]Advanced Mining Technology Center, Universidad de Chile, Avenida Tupper 2007, Santiago 8370450, Chile
[4]GeoExpedition, Las Palomas 25, Pirque, Santiago 9480000, Chile
[5]Institute of Geochemistry and Petrology, Department of Earth Sciences, ETH Zürich, 8092 Zürich, Switzerland
[6]Andean Geothermal Center of Excellence CEGA, Universidad de Chile, Plaza Ercilla 803, Santiago 8370450, Chile

ABSTRACT

Crystal-melt separation has been invoked as a mechanism that generates compositional variabilities in magma reservoirs hosted within the Earth's crust. However, the way phase separation occurs within such reservoirs is still debated. The San Gabriel pluton of central Chile is a composite pluton (12.82 ± 0.19 Ma) with wide textural/compositional variation (52–67 wt% SiO_2) and presents a great natural laboratory for studying processes that occur in upper crustal magma reservoirs. Geochemical and geochronological data supported by numerical models reveals that shallow magma differentiation via crystal-melt separation occurred in magma with intermediate composition and generated high-silica magmas and cumulate residues that were redistributed within the reservoir.

The pluton is composed of three units: (1) quartz-monzonites representing the main hosting unit, (2) a porphyritic monzogranite located at the lowest exposed levels, and (3) coarse-grained quartz-monzodiorites with cumulate textures at the middle level of the intrusive. Calculations of mass balance and thermodynamic modeling of major and trace elements indicate that <40 vol% of haplogranitic residual melt was extracted from the parental magma to generate quartz-monzonites, and 50–80 vol% was extracted to generate quartz-monzodiorites, which implies that both units represent crystal-rich residues. By contrast, the monzogranites are interpreted as a concentration of remobilized residual melts that followed 30–70 vol% fractionation from a mush with 0.4–0.55 of crystal fraction. The monzogranites represent the upper level of a pulse that stopped under a crystal-rich mush zone, probably leaving a mafic cumulate zone beneath the exposed pluton. This case study illustrates the role of the redistribution of residual silicic melts within shallow magma reservoirs.

INTRODUCTION

Magma transport and the evolution of intermediate to felsic crustal magmatism have been intensively debated, motivated by questions about how crustal magmas are emplaced, feed volcanic eruptions, and modulate the compositional differentiation of the continental crust (e.g., Marsh, 1989; Petford et al., 2000; Vigneresse, 2006; Miller et al., 2009; Bachmann and Huber, 2016; Cashman et al., 2017). Despite the widespread agreement about incremental growth of shallow magma reservoirs (e.g., Lipman, 2007; Miller, 2008; Žák et al., 2009; Farina et al., 2010; Frazer et al., 2014; Gray et al., 2008), crucial aspects of the internal evolution of such reservoirs remain unclear. In particular, the plutonic record of silicic magma generation within crystal-rich magma reservoirs in the upper crust has been addressed by numerous studies (Lee et al., 2015; Fiedrich et al., 2017; Bachmann and Huber, 2019; Barnes et al., 2016; Schaen et al., 2018). However, textural, geochemical, and numerical/thermodynamical modeling studies, both at a large regional scale and applied to single plutons, suggest that most intermediate to silicic plutonic rocks represent cumulates that lose significant amounts of interstitial melt (e.g., Barnes et al., 2019; Cornet et al., 2022).

Some studies carried out on upper crustal plutons indicate that the predominantly cold temperatures in the upper crust result in rapidly crystallized early pulses that inhibit the formation of melt-rich magma reservoirs at shallow crustal levels (Glazner et al., 2004; Matzel et al., 2006), although these works ignore the evidence for thermal maturation of the shallow crust during the development of shallow crustal plutons (see, e.g., Bachmann et al., 2007; de Silva and Gregg, 2014). Homogenization of upper crustal reservoirs would be limited by the high effective viscosity of highly crystalline silicic magmas under these conditions and the marked rheological changes between mafic and felsic magmas (Scaillet et al., 1998; Jellinek and Kerr, 1999; Laumonier et al., 2014; Putirka et al., 2014). In this interpretation, shallow magma reservoirs are pictured as relatively static systems with scarce internal dynamics, compositional homogenization, and convective stirring. The compositional diversity preserved in intermediate and felsic plutons would thus not form at the emplacement level but be inherited from deeper reservoirs, where magma differentiation and the production of intermediate-silicic magmas occur (McNulty et al., 1996; Coleman et al., 2004, 2012; Michel et al., 2008; Žák et al., 2009; Jacob et al., 2015).

Italo Payacan https://orcid.org/0000-0002-2198-709X

In contrast, other studies provided evidence that upper crustal magma reservoirs are more dynamic, including episodes of melt extraction (Weinberg, 2006; Webber et al., 2015; Barnes et al., 2016; Fiedrich et al., 2017; Hartung et al., 2017; Garibaldi et al., 2018; Holness, 2018; Tavazzani et al., 2020) and reactivation-rejuvenation of high-crystallinity magmas triggered by hot magma recharges (Mahood, 1990; Wiebe et al., 2004; Sliwinski et al., 2017; Brahm et al., 2018). The internal architecture and magmatic structures preserved in plutonic bodies are commonly interpreted as evidence of magmatic stirring and mingling between basic and acid magmas (e.g., Leuthold et al., 2012; Putirka et al., 2014). The existence of density instabilities and convective currents could favor "magmatic recycling" (Paterson et al., 2008; Paterson, 2009) and internal rheological contrasts affecting the magma reservoir dynamics (Paterson and Miller, 1998; Hawkins and Wiebe, 2004; Paterson et al., 2012). This interpretation supports the idea that shallow magma reservoirs are active systems where younger intrusions may interact with mushy zones formed by older pulses, eroding and reworking the previously emplaced material (Bergantz, 2000; Bachmann et al., 2007; Walker et al., 2007; Miller et al., 2011; Paterson et al., 2016). Those processes may be expressed in the internal contacts and complexities between textural and compositional domains in plutons (Paterson et al., 1998; Bergantz, 2000).

Many observations suggest that internal differentiation processes of shallow magma reservoirs can occur in a crystal-rich mush state when residual silicic melts are extracted (see a review in Bachmann and Huber, 2019). Those melts may be extracted and transported to upper crustal levels or redistributed within the reservoir, giving rise to caps of potentially eruptible, crystal-poor magma (Lindsay et al., 2001; Bachl et al., 2001; Hildreth and Wilson, 2007; Bachmann and Bergantz, 2008; de Silva and Gregg, 2014; Aravena et al., 2017; Karakas et al., 2017). The identification of crystal cumulate zones in upper crustal plutons has been supported by whole-rock geochemistry (Bachl et al., 2001; Deering and Bachmann, 2010; Gelman et al., 2014; Lee and Morton, 2015; Aravena et al., 2017; Schaen et al., 2017) and textural features (Vernon and Collins, 2011; Fiedrich et al., 2017; Garibaldi et al., 2018; Holness, 2018). Trace element variability in plutons has been widely used to reproduce residual melt segregation processes and identify the solid-rich cumulate from which melts were extracted (Deering and Bachmann, 2010; Lee and Bachmann, 2014). Trace element signatures in felsic cumulates are not always easy to interpret, though, because of the partition coefficient variations of the phase crystallization sequence (Gelman et al., 2014) and the limited melt extraction efficiency due to crystallinity and terminal porosity in shallow magma chambers (Dufek and Bachmann, 2010; Lee and Morton, 2015).

Previous studies of Miocene intermediate–silicic Andean plutons have highlighted crystal-melt separation as a mechanism to explain compositional and textural heterogeneities. One example is the La Gloria pluton (Mahood and Cornejo, 1992; Cornejo and Mahood, 1997; Gutiérrez et al., 2013; Payacán et al., 2014; Aravena et al., 2017), a neighboring Miocene body located north of the San Gabriel pluton of central Chile. The La Gloria pluton is much more homogeneous in texture and composition (61–65 wt% SiO_2) and has cryptic internal contacts (Cornejo and Mahood, 1997; Aravena et al., 2017). On the other hand, the Rico Bayo–Huemul plutonic complex (35°S) offers a more complete record of a magma reservoir where silicic residual melts were redistributed to generate the compositional zonation, recording the complementary crystal cumulate of the fractionation process (Schaen et al., 2017; Garibaldi et al., 2018). These cases probably provide evidence for the generation of rhyolitic magmas in the upper crust.

In this contribution, we present the case of the San Gabriel pluton of central Chile, an example of an epizonal magma reservoir that displays wide compositional and textural variations. A magmatic evolution is proposed based on a combination of petrographic geochemical (bulk-rock composition) data, U-Pb dating, and thermodynamic and trace element modeling. Through this case study we document a shallow (upper crustal) fossil magma reservoir where the compositional variability is explained by in situ magma reservoir processes controlled by crystal-melt separation from a mush with intermediate composition (differing from a process sustained over time such as crystal settling). The products were redistributed within the reservoir as cumulates with intermediate composition (crystal-rich residue resulting from the extraction of all or part of the haplogranitic interstitial melts) or as the accumulation levels of silicic crystal-poor magmas that were extracted from mushy magmas, generating dacitic to rhyolitic magmas.

GENERAL BACKGROUND OF THE SAN GABRIEL PLUTON

The San Gabriel pluton is an upper Miocene (ca. 11.5 Ma; Ar-Ar dates; Kurtz et al., 1997) intrusive body of ~40 km^2 of areal exposure that is located in the northern part of the Southern Volcanic Zone in the Andes of central Chile (Fig. 1A). It was shallowly emplaced (roof at ~4–5 km depth, similar to the neighboring La Gloria pluton; Cornejo and Mahood, 1997; Gutiérrez et al., 2018), intruding volcanosedimentary rocks (Abanico and Farellones Formations, Eocene–Oligocene to lower Miocene and lower Miocene to middle Miocene, respectively) at the eastern half of an Eocene–Oligocene to Miocene intra-arc basin (Thiele, 1980; Charrier et al., 2002; Fock, 2005). The evolution of the basin was characterized by a period of intense crustal deformation and thickening accompanied by volcanism that progressively differentiated with time and was dominated by dacitic-rhyolitic compositions in the late stage (Nyström et al., 2003). In this scenario, the San Gabriel pluton was emplaced as part of an ~40-km-wide Miocene subduction-related plutonic belt, trending north–south and consisting of discrete quartz-monzodioritic plutons (Fig. 1A), which tend to be younger on the eastward side (Muñoz et al., 2013). These plutons' emplacement was favored by the presence of long-lived crustal high-permeability zones associated with the intersections of fault systems oblique to the arc (Piquer et al., 2015, 2016), and some of them are related to the formation of giant porphyry-type ore deposits (Teniente and Río Blanco–Los Bronces districts; Deckart et al., 2010; Piquer et al., 2015).

Rapid Tertiary–Quaternary uplift, exhumation, and glacial erosion has exposed as much as

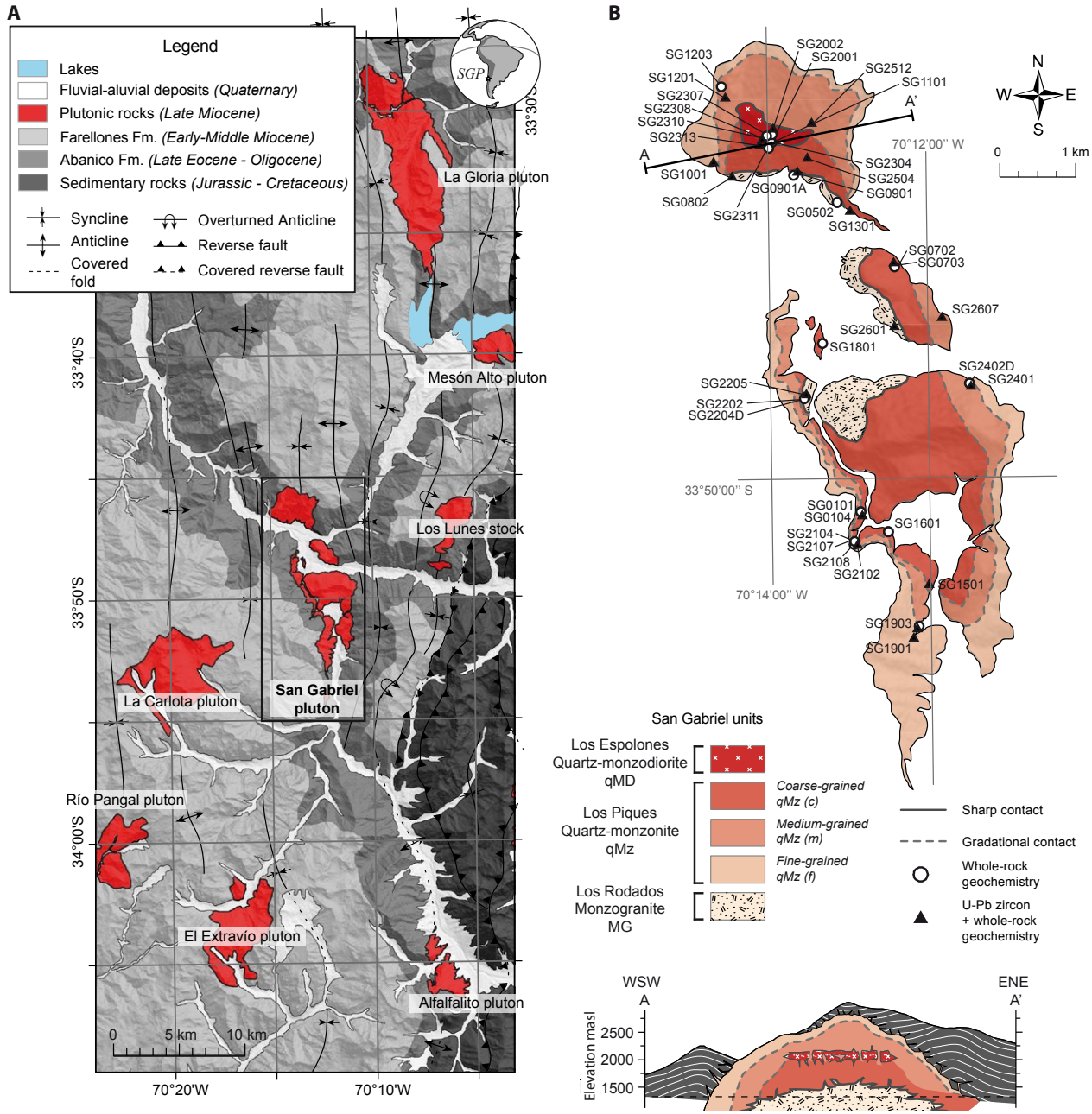

Figure 1. (A) Geological map shows the Miocene plutonic belt, to which the San Gabriel pluton belongs. Based on Thiele (1980) and Fock (2005). (B) Lithological map and cross-sections of the San Gabriel pluton show the units defined in this study. Color scale indicates the silica content of each unit (red is the most mafic, whereas light pink is the most felsic). qMD—quartz-monzodiorite; qMz—quartz-monzonite; MG—monzogranite. White circles show the locations of samples with whole-rock geochemistry. Black circles show the locations of samples analyzed for petrography, whole-rock composition, and U-Pb zircon dating (coordinates appear in Table S1, see text footnote 1). masl—meters above sea level.

1000 m of vertical relief in the pluton, which facilitates recognition of borders, interior zones, and the roof (Fig. 2; Farías et al., 2008; Muñoz-Gómez et al., 2020). The San Gabriel pluton is an elongate laccolith that is 12 km long and 3 km wide and situated in a N30°W direction (Fig. 1B), where steeply dipping lateral walls and some subhorizontal parts of the roof can be observed (Fig. 2A). The pluton presents an irregular shape, with some apophyses in the contacts, so that the largest vertical section is observed at the northern end (up to 1000 m), where the roof is exposed. The contact between the San Gabriel pluton and its volcanic host rocks is mainly sharp with a stepped geometry (Fig. 2). Locally, some decimeter-wide dikes invading the host volcanics are observed close to the contact, and many isolate some wall-rock blocks (Figs. 2D and 2E).

SAN GABRIEL PLUTON PETROGRAPHIC FEATURES

Magmatic Units

Zoning of the San Gabriel pluton consists of vertical and concentric variations in mineral modes, textures, grain size, and color index (Fig. 1B). The San Gabriel pluton is mostly composed of quartz-monzonite and quartz-monzodiorite, although a wide range of magmatic facies are distinguishable, which vary from quartz-diorite up to monzogranite (Fig. 3). The main minerals are plagioclase, K-feldspar, quartz, biotite, and hornblende (pyroxenes are sparsely present), while titanite, apatite, zircon, and Fe-Ti oxides are accessory minerals. The rocks that comprise the pluton are mainly equigranular and medium- to coarse-grained, although fine-grained and porphyritic textures are also observed. Three magmatic units are distinguished by their modal mineralogy: the Los Piques quartz-monzonite, the Los Espolones quartz-monzodiorite, and the Los Rodados monzogranite. There are sharp inter unit contacts, arranged such that the Los Piques quartz-monzonite (the main one) hosts the Los Espolones quartz-monzodiorite and Los Rodados monzogranite (Fig. 1B).

Los Piques Quartz-Monzonite

This unit makes up most of the pluton and corresponds to equigranular quartz-monzonite with biotite and minor hornblende, which encompasses the marginal and inner parts, where some quartz-monzodiorite appears. Three subunits are distinguished by different grain sizes, which are distributed concentrically and vary continuously from coarse-grained in the internal zone to fine-grained toward the borders and show gradational contacts (Figs. 1B and 3).

Los Piques quartz-monzonite, composed of euhedral plagioclase (35–45%), subhedral to anhedral K-feldspar (10–25%), anhedral quartz (5–20%), and euhedral biotite (10–15%), generally replaces hornblende (5–12%), which is altered to actinolite, and minor clinopyroxene (0–5%; Fig. 3). Many quartz and K-feldspar crystals are interstitial, filling the spaces between euhedral plagioclase crystals. Hornblende is often present as clusters with biotite and Fe-Ti oxides, which are also present as inclusions within hornblende crystals. Seriate texture principally appears in plagioclase, especially in the marginal fine-grained facies.

Los Espolones Quartz-Monzodiorite

This unit is composed mainly of plagioclase-rich, coarse-grained quartz-monzodiorite (even some quartz-diorite; Fig. 3E) and is observed in the middle level of the northern part of the San Gabriel pluton. Many centimeter- to decimeter-sized blocks from the Los Espolones quartz-monzodiorite are enclosed in Los Piques quartz-monzonite (Fig. 4A).

The Los Espolones quartz-monzodiorite is exposed as a subhorizontal layer that presents sharp contacts with the Los Piques unit. The modal mineralogy consists of euhedral plagioclase (42–65%), K-feldspar (10–15%), and anhedral quartz (5–8%), and a higher color index compared to the rest, reaching up to 35% mafic minerals, including hornblende (7–13%), biotite (5–11%), clinopyroxene (2–7%), and Fe-Ti oxides (2–5%; Fig 3E). Texturally, the Los Espolones quartz-monzodiorite presents mesocumulate textures in plagioclase, where euhedral crystals in contact between them are observed, forming a crystal network with interstitial mafic minerals, K-feldspar, and quartz (Fig. 3E). Kink folds are occasionally observed in plagioclase crystals, which indicates that solid-state deformation affected the crystal network.

Los Rodados Monzogranite

Los Rodados monzogranite occupies subhorizontal bodies (lens shape) in lower levels of the San Gabriel pluton (Fig. 1B). It is composed of an amalgamation of medium-grained and porphyritic pink facies, felsic dikes, and pockets of medium- to fine-grained monzogranite that show both sharp and diffuse contacts. This unit presents sharp and irregular contacts, with many porphyritic dikes intruding the Los Piques quartz-monzonite (Figs. 4B and 4C), which indicates that the Los Rodados monzogranite is younger than the host quartz-monzonite.

The modal mineralogy of the Los Rodados monzogranite consists of medium to coarse euhedral plagioclase (20–35%), subhedral to anhedral K-feldspar (25–35%), and quartz (15–25%). Mafic phases are hornblende (6–9%), biotite (3–6%), Fe-Ti oxides (2–5%), and minor clinopyroxene (0–3%). The Los Rodados monzogranites generally exhibit variable plagioclase phenocryst content (50–80%) surrounded by K-feldspar, quartz, less plagioclase, and ferromagnesian minerals (Fig. 3F). Interstitial hornblende and K-feldspar appear in some samples.

Magmatic Structures

Aplitic leucogranitic dikes and pockets are preserved in the San Gabriel pluton, varying from 0.5 cm to 10 cm wide, and associated K-feldspar pegmatites and some miarolitic cavities are also found (Figs. 4C and 4D). Dikes are medium- to fine-grained with biotite + hornblende + titanite + Fe-Ti oxides, and they occur mainly in the Los Rodados monzogranite and sparsely in the upper levels of Los Piques quartz-monzonite.

Some concentration bands of ferromagnesian minerals are occasionally observed in the San

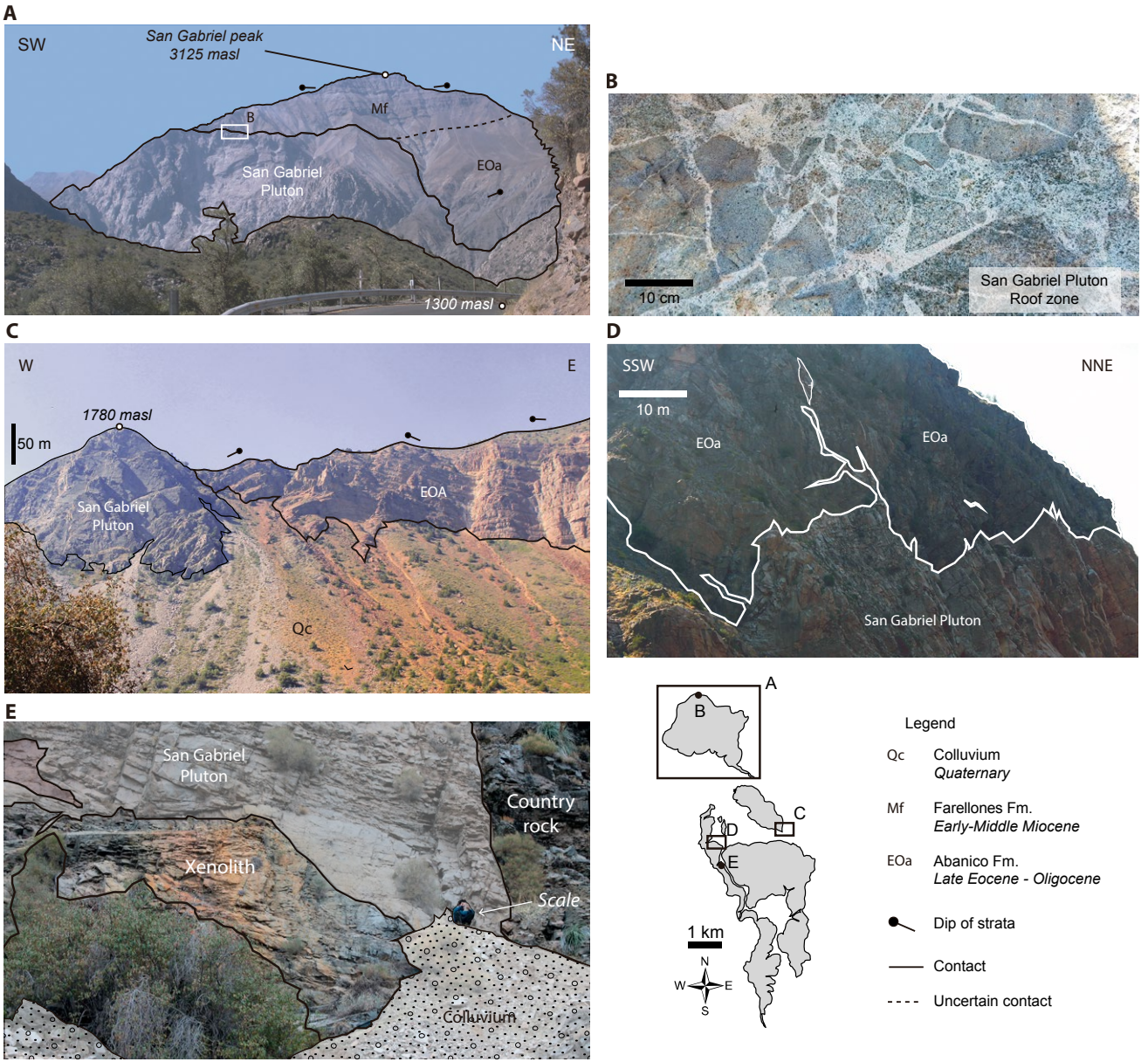

Figure 2. Field views of the San Gabriel pluton contacts with the host volcanic rocks show the structural relationship. (A) View of the northern end of the pluton, where the major exposure is observed (~1 km). (B) Outcrop of host-rock blocks preserved near the roof of the pluton in the northern part. (C) Eastern contact, where strata are oblique to the pluton contact. (D) South-western contact exhibits a steep and irregular shape, with some dikes intruding into the host rock, which suggests brittle mechanical behavior during the intrusion. (E) Xenolith preserved in the western contact of the San Gabriel pluton. masl—meters above sea level.

Gabriel pluton, mainly within the coarse facies of the quartz-monzonite (Figs. 4E and 4F). Structures of this type are characterized by the concentration of biotite and amphibole crystals from the quartz-monzonitic facies. In general, these mafic mineral concentration bands vary in size between a few centimeters to decimeters, and are open, asymmetrical, and slightly graded in mafic mineral contents (Fig. 4F). Both subhorizontal and subvertical orientations are observed, resembling schlieren-bounded troughs, which are thought to be evidence of magmatic flow channels or rheology contrasts in the magmatic reservoir that are analogous to sedimentary bedforms (Paterson, 2009).

Mafic enclave-rich layers appear at middle levels of the San Gabriel pluton and are associated with internal contacts between textural units, especially above the Los Espolones quartz-monzodiorite; they coexist with straight-shaped blocks. The concentration of mafic enclaves is also observed within the Los Piques quartz-monzonite, which is elongated and oriented with a NW trend that is parallel to the pluton walls. Some zones present a high concentration of mafic enclaves covering more than 60%

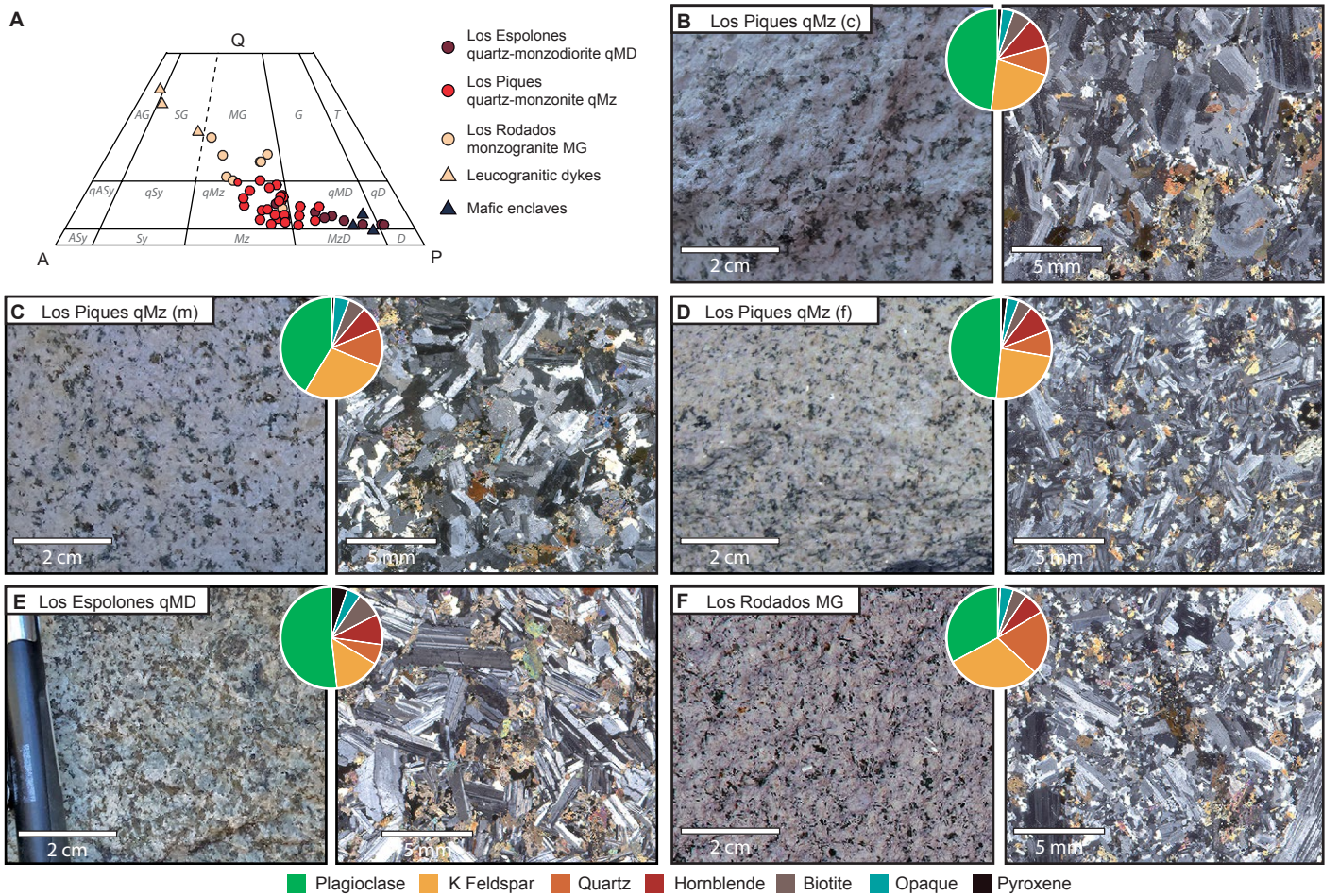

Figure 3. (A) Ternary plot (Streckeisen, 1974) with the modal mineral content of rocks comprising the San Gabriel pluton (Q—quartz; A—alkaline feldspar; P—plagioclase). (B–F) Field photographs of rocks and photomicrographs in cross-polarized light of representative samples of San Gabriel pluton units. Pie charts show the representative modal content of major minerals. Samples from coarse (c), medium (m), and fine-grained (f) facies of the Los Piques quartz-monzonite are distinguished. qMD—quartz-monzodiorite; qMz—quartz-monzonite; MG—monzogranite.

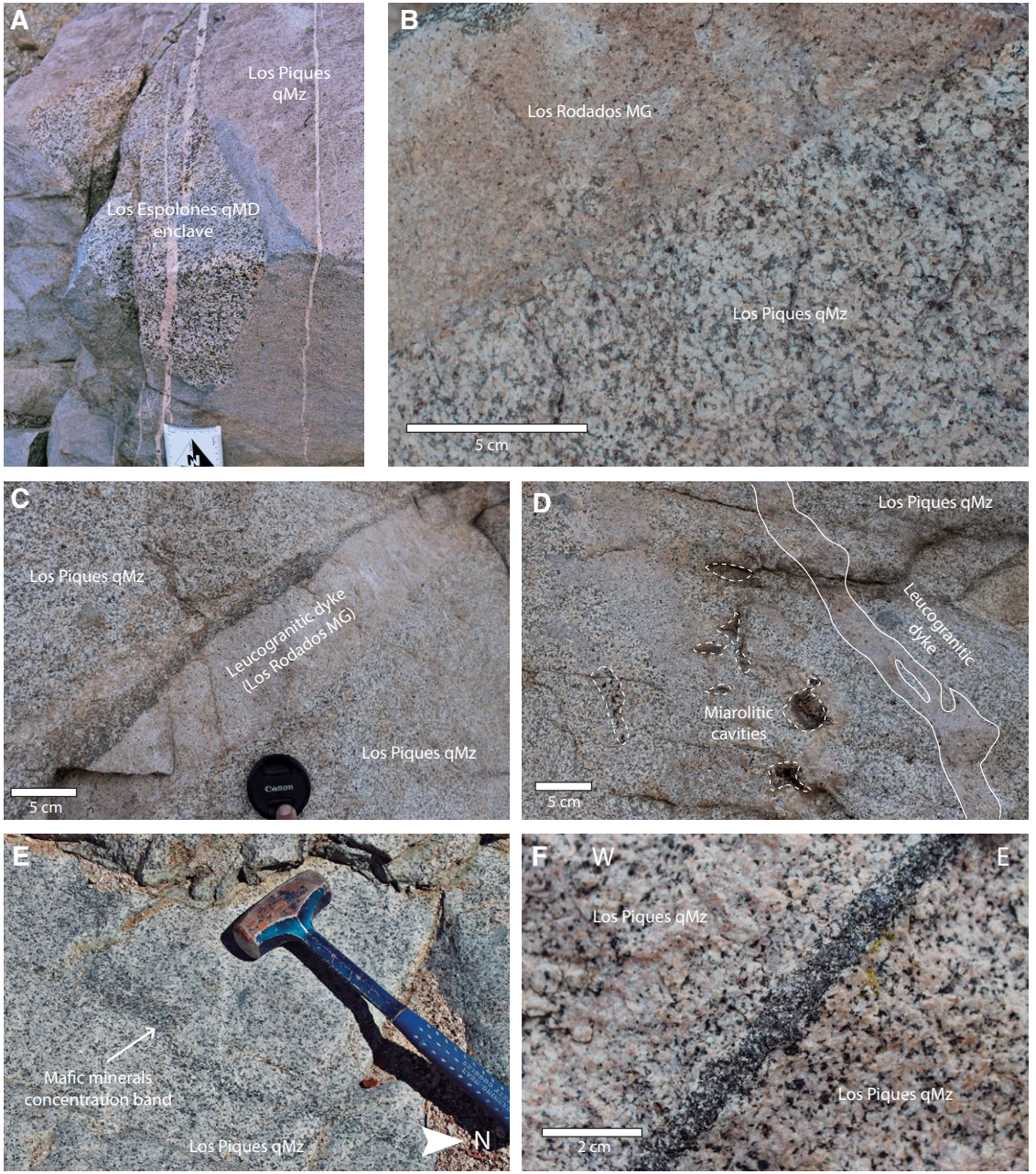

Figure 4. Field photographs of magmatic contacts and structures observed in the San Gabriel pluton are shown. (A) Enclave of mafic coarse-grained Los Espolones quartz-monzodiorite surrounded by the medium-grained Los Piques quartz-monzonite (qMz), which are observed at the intermediate level of the San Gabriel pluton. (B) Magmatic contact between the Los Piques quartz-monzonite and the porphyritic Los Rodados monzogranite (MG). Crystals from quartz-monzonite are cut by the monzogranite. (C–D) Leucogranitic dikes (inferred as coming from the Los Rodados monzogranite) intrude the Los Piques quartz-monzonite. They commonly exhibit pegmatitic K-feldspar and biotite plus anhedral quartz. Miarolitic cavities are marked in panel D, which contain quartz and K-feldspar crystals and are spatially associated with leucogranitic dikes. (E) Biotite and amphibole concentration zone with subhorizontal disposition within the Los Piques quartz-monzonite. (F) Mafic mineral concentration bands (schlieren-like) disposed in a subvertical plane within the Los Piques quartz-monzonite, where a slightly increasing mafic phase content appears toward the east. qMD—quartz-monzodiorite.

of the outcrop. These data are outside the scope of this paper, but additional information can be found in the Supplemental Material[1].

ANALYTICAL METHODS

Major elemental whole-rock composition analyses were performed on 30 samples by X-ray fluorescence (XRF) spectrometry on fused glass-beads with a PANalytical Axios XRF spectrometer at the ETH Zürich Institute of Geochemistry and Petrology. Rocks were crushed in an agate mill. The limit of detection was lower than 0.01 wt% for each oxide. Standard and rock sample-fused glass beads were prepared from rock powder mixed with lithium-tetraborate using a Claisse M4 fluxer. Trace element whole-rock composition analyses were determined by laser ablation–inductively coupled plasma–mass spectrometry (LA-ICP-MS) at the Institute of Geochemistry and Petrology of ETH Zürich, by analyzing the XRF glass beads using an ArF excimer laser coupled with an Elan 6100 DRC PerkinElmer. Three spots with a diameter of 90 µm were measured from each sample. NIST SRM 610 was used as standard reference material. Data were reduced by using SILLS (Guillong et al., 2008), where CaO concentrations obtained by XRF measurements were used as the internal standard.

U-Pb LA-ICP-MS geochronological analyses of zircons were carried out on 20 samples, covering all of the magmatic units of the San Gabriel pluton. Zircons were separated by routine procedures of mechanical separation methods (Gemini table), magnetic separation, and decantation in heavy liquids, both in the sampling and mineral separation laboratory of the Geology Department of the University of Chile, Santiago, Chile, and the Institute of Geochemistry and Petrology at ETH in Zurich, Switzerland. Zircons were mounted in epoxy resin and then polished, with ~60 crystals per sample. Crystals were characterized by cathodoluminescence imaging obtained using a SEM Quanta 200S (10 kV) in the Microscopy Laboratory of the Institute of Geochemistry and Petrology at ETH Zurich, Switzerland.

Zircon dating was performed in the Isotope Geochemistry and Cosmochemistry Laboratory at ETH Zurich. An ASI (Resonetics) RESOlution S115 laser ablation system was used with 193 nm of wavelength and ~2 J/cm^2 fluence. The ablation duration was 40 s, with a repetition rate of 5 Hz and a gas carrier compound comprising 100% He with 0.7 l/min flows. The laser system was connected to a Thermo Scientific Element XR single collector ICP-MS (1400–1550 W). Zircon data were obtained from ~60 spots per sample, with a size of 30 µm and ~16 µm depth (0.08 s each pulse). Standardization and drift-corrections for zircon dates were applied with the GJ-1 and 91500 standards, whereas the NIST SRM 610 standard was utilized for zircon composition. Data reduction and drift-correction were carried out using Iolite V2.5 (Paton et al., 2011). Ages and error calculations were carried out with Isoplot 4.15 (Ludwig, 2008) by using a weighted mean based on the uncertainty (2σ). Spots with clear Pb loss were disregarded. The method utilized in this study allows uncertainties of up to 1% 2σ to be obtained on weighted mean dates (Guillong et al., 2016; Sliwinski et al., 2017), which represents an approach to determine cooling patterns within 10 Ma plutons, if differences are lower than 200 ka (Gutiérrez et al., 2018).

WHOLE-ROCK GEOCHEMISTRY

Major Elements

The San Gabriel pluton has a wide and continuous compositional range, from 52 wt% to 68 wt% SiO_2 on an anhydrous basis, except for three leucogranitic dikes with ~75 wt% SiO_2 (Figs. 5A and 5B; data set is presented in Table S1, see footnote 1). Variations in the Pearce element ratio based on the feldspar stoichiometry indicate that the magmatic units were controlled mainly by feldspar fractionation (Ni was used as a conservative element because of the small amount, if any, of olivine as cumulates; Fig. 6). The Los Espolones quartz-monzodiorites are the most basic rocks with 52–55 wt% SiO_2. The Los Piques quartz-monzonites have 56–64 wt% SiO_2, whereas the Los Rodados monzogranites have 64–68 wt% SiO_2. Al_2O_3, TiO_2, FeO_t, MgO, CaO, and P_2O_5 concentrations tend to decrease linearly with silica content, whereas K_2O content increases linearly with silica abundance. Na_2O behavior varies according to the magmatic unit: it tends to increase with silica content for the quartz-monzodiorites and quartz-monzonites and decreases for the monzogranites and leucogranitic dikes, exhibiting an inflection point at around 63 wt% SiO_2 (Fig. 5B).

Trace Elements

Rocks from the San Gabriel pluton show well-defined patterns in whole-rock trace element content (Fig. 7; Tables S1 and S2, see footnote 1). Sr and Sc content decreases as SiO_2 content increases, whereas Rb increases with SiO_2 concentration (Fig. 7). Other trace elements, such as Ba, Y, La, and Zr show variations from an increasing trend for quartz-monzodiorites and some quartz-monzonite samples to decreasing trends for samples with more than 60 wt% SiO_2, exhibiting an inflection close to the most siliceous samples from Los Piques quartz-monzodiorite (Fig. 7). However, two samples with SiO_2 around 65 wt% (part of the Los Rodados monzogranite) are enriched in those elements and show concentrations consistent with the compositional trends of the less siliceous samples. Interestingly, an inflection around 61 wt% SiO_2 is observed in the Rb concentration, coincident with the transition from quartz-monzodiorites and quartz-monzonites (steep trend) to monzogranites and leucogranites (smoother trend; Fig. 7).

[1]Supplemental Material. Table S1: XRF whole-rock geochemistry. Table S2: LA-ICP-MS whole-rock trace elements data. Table S3: LA-ICP-MS results of trace element concentrations. Table S4: Individual spot measurements obtained via LA-ICP-MS on zircon crystals. Supplemental text with Table S5, Table S6, Figure S1, Figure S2, Figure S3, Figure S4, Figure S5, and Figure S6. Please visit https://doi.org/10.1130/GEOS.S.21893064 to access the supplemental material, and contact editing@geosociety.org with any questions.

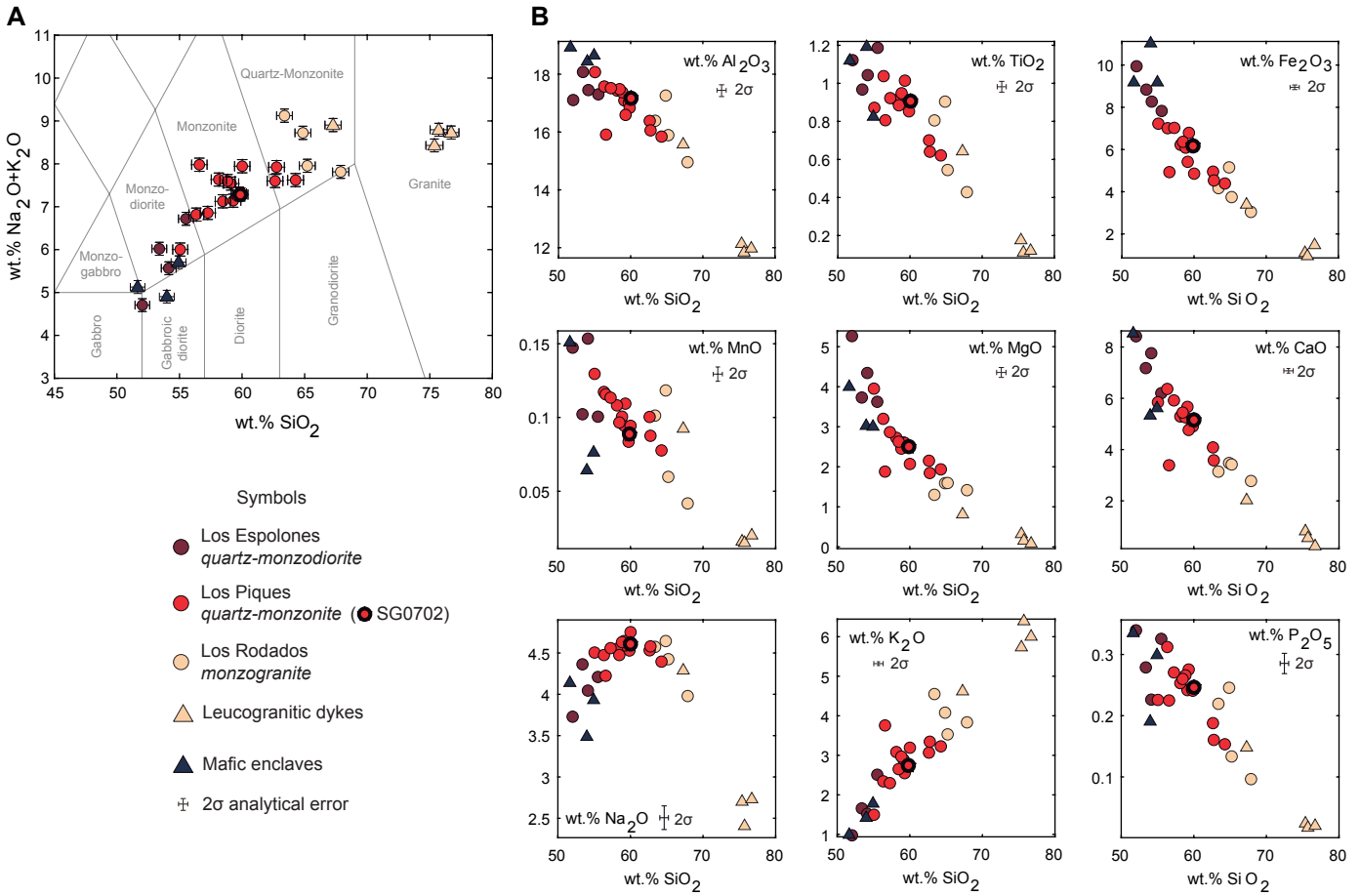

Figure 5. Plots show major element variations of the whole-rock units of the San Gabriel pluton and associated rocks (mafic enclaves and leucocratic dikes) obtained through X-ray fluorescence (XRF) analyses. (A) Total alkali versus silica (TAS) diagram (Middlemost, 1994) and (B) binary plots of silica versus major and minor elements (2σ analytical error is smaller than symbol size and presented with a referential size).

U-Pb ZIRCON GEOCHRONOLOGY

Zircon dates of all samples give a weighted mean age of 12.82 ± 0.19 Ma, exhibiting a Gaussian distribution (N = 1743) and a significant dispersion with a mean square of weighted deviates (MSWD) = 4.3. Weighted ages of individual samples vary between 12.41 ± 0.20 Ma and 13.57 ± 0.23 Ma (Figs. 8 and S2; see footnote 1), and no important Pb loss was recognized. All spots show ages younger than 30 Ma (see Tables S3 and S4, footnote 1).

Zircon dates of individual samples mostly show variable dispersions, with MSWD values between 1.01 and 3.8. Sample SG0104, which belongs to Los Piques quartz-monzonite and presents the coarser zircon crystals, has an MSWD of 5.4 (Fig. 8). The difference between the maximum and minimum ages, considering the major and lower 2σ limit of confidence, indicates a maximum lifetime of 1.56 Ma for magma reservoir crystallization. The weighted ages are similar for all the samples, and most of them overlap with the global mean and confidence interval (12.82 ± 0.19 Ma). Samples SG0702, SG2504, and SG2601 are exceptions. These samples, with ages older than that of the global mean, are located at the eastern side of the pluton and are interpreted to represent early stages of magmatism.

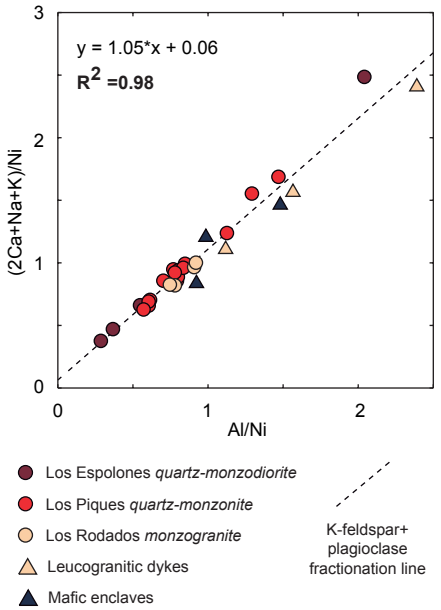

Figure 6. Pearce element ratio (PER) diagram constructed according to the feldspar stoichiometry and using Ni as a conservative element.

GEOCHEMICAL MODELING: METHODOLOGY

To further explore the cumulate and residual silicic melt signatures of each magmatic San Gabriel pluton unit, geochemical simulations of major and trace elements were carried out. Through these simulations, we quantified the volume fraction of trapped silicic melt within each unit, showing that the compositional variation of the pluton can be generated via crystal-melt separation and redistribution. In this model, each composition was chemically reproduced by a combination of residual liquids and solid-phase compositions in different proportions. This does not mean that a unit came entirely from another unit through a unique differentiation event, but rather that each unit was formed from a single crystallization sequence arising from a common parental magma from which liquids and crystals were reorganized in different proportions (with crystals or interstitial melts removed from both). This can occur either in situ in the reservoir or by different pulses arising from a common source from deeper levels of the reservoir (or the crust). However, the relatively high solid contents required in this mass balance, and the content of euhedral crystals in the quartz-monzodiorites, indicate that mafic magmas were crystal-rich, which prevented magma flow through the system because of the high effective viscosity. This, in combination with the superposition of different units' ages, supports our assertion that separation and remobilization processes at the emplacement level are more reasonable than a completely pulse-dominated model.

Geochemical simulations include three steps. First, the crystallization sequence and the phase compositions (solid and melts) were modeled from cooling of the parental magma. Second, the partition of trace elements (Rb, Sr, and Zr) is simulated to evaluate their distribution in the cumulate and residual melts by using the phase equilibria. Third, a mass balance between the simulated compositions of solid phases and residual melts is carried out to reproduce the major element concentrations of each San Gabriel pluton sample. This step allowed us to quantify the amount of melt that was removed in the case of cumulates, or crystals that were fractionated in the case of samples that are interpreted as concentrations of silicic melts. Details of the simulation steps are explained in the following sections.

Thermodynamical Modeling of the Crystallization Sequence of the Parental Magma

To reproduce San Gabriel pluton compositions, we assume that parental magma is recorded in the Los Piques quartz-monzonites, supported by the fact that it hosts the rest of the units and lacks cumulate textures as compared to the Los Espolones quartz-monzodiorites. For modeling purposes, we consider the parental magma composition to be equivalent to that of sample SG0702, which corresponds to a coarse-grained quartz-monzonite of hornblende (8%) and biotite (6%; Fig. 3B), with 59.74 wt% SiO_2 content (Table S5; see footnote 1). SG0702, one of the oldest samples from the Los Piques unit (Fig. 8), is located close to the eastern pluton border, which suggests it could represent the early magmas during the construction of the reservoir.

The modal crystallization sequence and residual melt composition were constrained via thermodynamical simulations of isobaric batch crystallization by using the rhyolite-MELTS version 1.0.2 software package (Gualda et al., 2012). Simulations considered a pressure of 1.5 kbar (consistent with the thickness of the overlying host rock), QFM+2 as oxygen buffer, and a water content of 4 wt%. All of these conditions are similar to those recorded in the neighboring Miocene La Gloria pluton (Gutiérrez et al., 2013). We tested whether changes in pressure and water contents (1 kbar, 1.5 kbar, and 2 kbar and 1 wt% H_2O, 2 wt% H_2O, and 4 wt% H_2O) have minor effects on the results (see Supplemental Material, footnote 1). Additionally, we determined that changes in physical condition do not significantly affect the simulated crystallinities and the calculated melt and solid compositions.

Modeling the Partitioning of Trace Elements

We analyzed Rb and Sr content variations in the San Gabriel pluton. These elements are highly sensitive to the crystallization of plagioclase, the most abundant mineral phase that seems to control the pluton crystallization sequence. The Sr and Rb contents in the San Gabriel pluton show a steep pattern in a Rb versus Sr diagram for samples with less than 61–63 wt% of SiO_2, whereas the more silicic Los Rodados monzogranite and leucogranitic dikes present a smoother pattern (Fig. 9A). Based on the study carried out by Gelman et al. (2014), the geochemical inflection observed at Rb/Sr = 0.5 could be interpreted as the change between a cumulate trend (steep) and an extracted residual melt trend (less steep), where plagioclase, hornblende, and biotite were fractionated. This study aims to show a suitable case where the calculated differences in trace elements between cumulate and extracted residual silicic melts are consistent with the first-order compositional observations and textural features of the pluton.

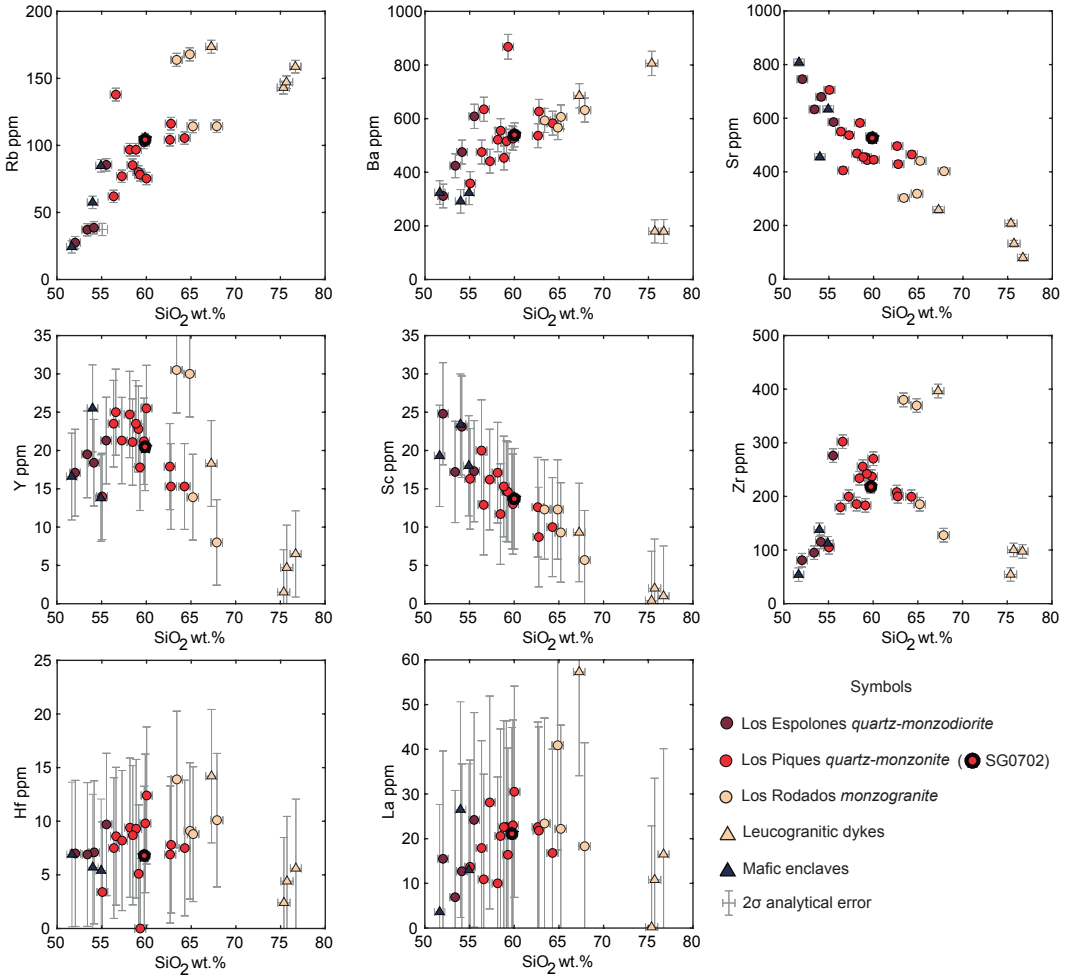

Figure 7. Binary plots of trace element variations versus silica content of the San Gabriel pluton units and associated rocks (mafic enclaves and leucocratic dikes) were obtained through X-ray fluorescence spectrometry and laser ablation–inductively coupled plasma–mass spectrometry.

To assess the Rb and Sr behavior during the segregation of residual melts and the associated cumulate, we assumed that the San Gabriel pluton was a closed system (scripts are available in the supplemental material of Gelman et al., 2014). We formulated a generalized quantitative model for trace element distribution in a mushy magma reservoir, including equations for the partitioning of trace elements in the extracted melts and cumulates, the bulk partition coefficients' crystallinity dependence, and the efficiency of the melt extraction. Other elements, such as rare earth elements (REE), were not considered in this analysis because their compatibility depends on minor phases that induce uncertainties.

With the scripts provided by Gelman et al. (2014), we calculated the bulk partition coefficients (D_i^{bulk}) of the element *i* from the simulated crystallization sequence, crystallinity, and volume fraction of each phase (Fig. 9B), through the expression:

$$D_i^{bulk} = \sum_{j=1}^{N} x_j \cdot \left(K_d\right)_i^j$$

where *N* is the total number of crystallized phases, X_j is the *j* phase molar fraction, and $\left(K_d\right)_i^j$ is the partition coefficient of element *i* in the *j* phase. The values of $\left(K_d\right)_i^j$ that we use were obtained from the literature and are presented in Table S6 (see footnote 1). The bulk partition coefficients vary between 1 and 8 for Sr and 0–0.2 for Rb, with increasing trends regarding magma crystallinity

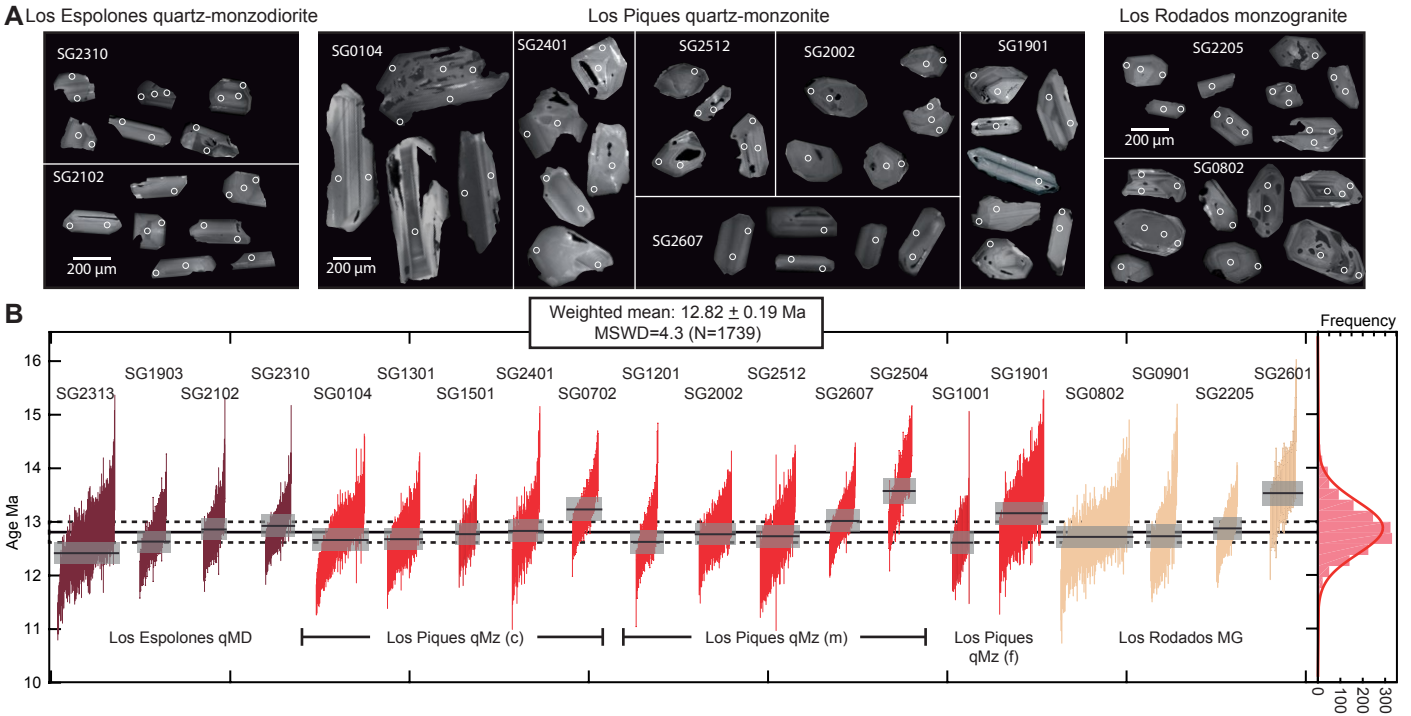

Figure 8. Laser ablation–inductively coupled plasma–mass spectrometry U/Pb zircon geochronology results from the San Gabriel pluton are plotted. (A) Cathodoluminescence images of the zircon crystals analyzed. Circles show the laser spots for U-Pb dating. (B) Rank-ordered $^{206}Pb/^{238}U$ zircon spot dates (2σ bars) with sample weighted means (2σ uncertainty). Samples from coarse-, medium-, and fine-grained facies of the Los Piques quartz-monzonite are grouped (c, m, and f, respectively). The histogram with the individual spot age frequency is shown on the right with vertical disposition. MSWD—mean square of weighted deviates; qMD—quartz-mozodiorite; qMz—quartz-monzonite; MG—monzogranite.

(Fig. 9C). However, the bulk partition coefficients for both elements present a narrow interval within the optimal crystallinity window for the extraction of interstitial melts (~60%; Dufek and Bachmann, 2010). Mean values of $D_{Rb}^{bulk} = 0.15$ and $D_{Sr}^{bulk} = 6.0$ for Rb and Sr were obtained (Fig. 9C).

The algorithm was set to model the distribution of the elements in equilibrium crystallization, and a Gaussian probability curve of residual melt extraction with a peak at the 60% of crystallinity (Dufek and Bachmann, 2010). For simplicity, we use the aforementioned values of Rb and Sr bulk partition coefficients. Extracted melt fractions of 0.1, 0.25, 0.5, and 0.8 were chosen to evaluate the phases' composition. Assimilation was neglected because its effect has not been recorded in the pluton.

The Zr partitioning is also modeled calculating the concentration in the residual melt at each temperature step (C_{Zr}), assuming the system remains zircon-undersaturated and Zr is ideally incompatible (red line in Fig. 10). The Zr concentration in the residual melt was calculated as:

$$C_{Zr} = \frac{mass\ of\ Zr\ in\ the\ initial\ sample}{mass\ of\ residual\ melt}.$$

The Zr content to reach the melt saturation in zircon was calculated based on the M parameter of the simulated melt composition ($M = [Na^{+}K+2Ca]/[Al \times Si]$) and the zircon saturation models (Watson et al., 2006; Lee and Bachmann, 2014; orange dotted line in Fig. 10). The intersection between the Zr content in evolved melts and the saturation curve represents the zircon saturation point, from which the melt is saturated in zircon and further fractionation processes will produce Zr-depleted magmas.

GEOCHEMICAL MODELING RESULTS

Parental Magma Crystallization Sequence

Thermodynamical simulations predict the early crystallization of pyroxene and accessory phases like magnetite, followed by plagioclase crystallization

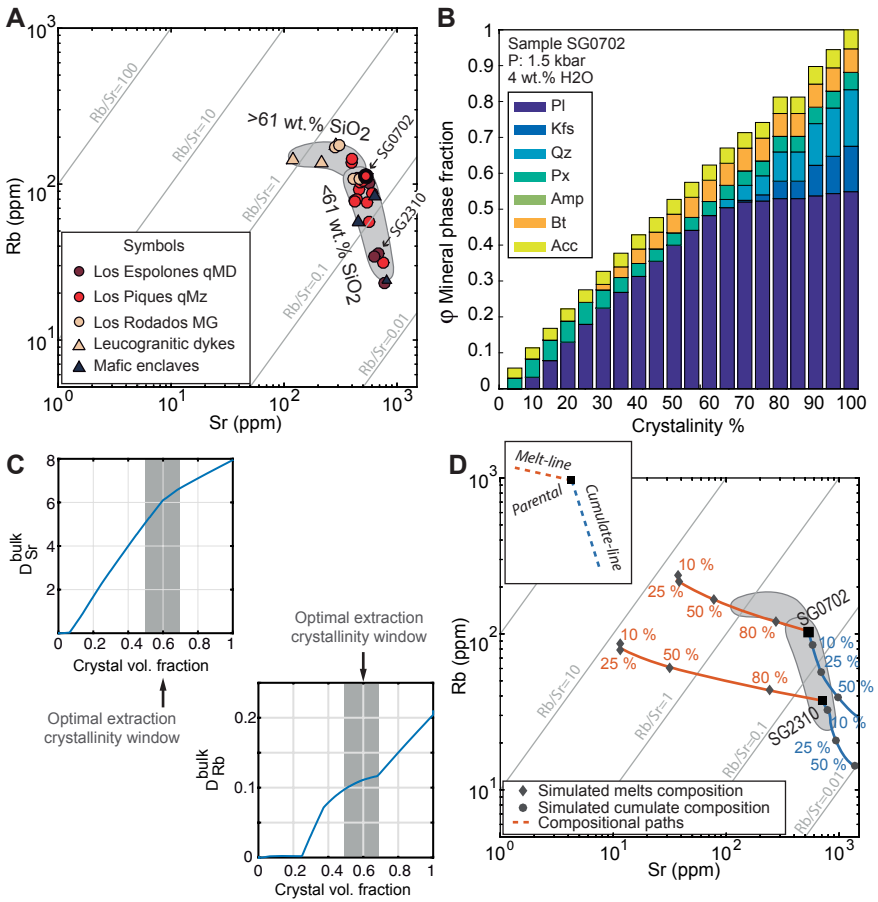

Figure 9. Geochemical modeling of San Gabriel pluton compositional variation. (A) Rb versus Sr content of the San Gabriel pluton. (B) Simulated volume fraction of the phases in equilibrium during San Gabriel pluton parental magma crystallization (SG0702), obtained via rhyolite-MELTS simulation (Pl—plagioclase; Kfs—K-feldspar; Qz—quartz; Px—pyroxene; Amp—amphibole; Bt—biotite; Acc—accessory phases as ilmenite and magnetite). (C) Variation of the bulk partition coefficient of Sr and Rb regarding the crystal volume fraction. The optimal extraction crystallinity window according to Dufek and Bachmann (2010) is highlighted in gray (0.5–0.7). (D) Rb and Sr partition modeling results following the formulation of Gelman et al. (2014) to track the trace element in the phases in a crystallizing magma. Black squares represent the starting points of intermediate (SG0702, ~60 wt% SiO_2) and basaltic magma (SG2310, ~52 wt% SiO_2) of the San Gabriel pluton. The compositions of simulated interstitial melt (orange) and the cumulate rocks (residual solids + trapped interstitial melts in blue) are presented, where percentages represent the total fraction of available interstitial melt that was extracted. qMD—quartz-mozodiorite; qMz—quartz-monzonite; MG—monzogranite.

when the magma reaches a crystal content of 10% (Fig. 9B). Biotite starts to crystallize at 30% crystallinity, while amphibole crystallization is subordinated, probably because pyroxene would be generated by rhyolite-MELTS as the equivalent phase (Gualda et al., 2012). Once 60% crystallinity was reached, late crystallization of quartz and K-feldspar took place in low modal concentrations, consistent with the quartz-monzodioritic to quartz-monzonitic mineral compositions of the Los Piques unit. See Supplemental Material (footnote 1) for simulations with diverse initial conditions of pressure and water content. Most major element contents show a linear trend with silica content, reproduced by unmixing processes, where the compositions of the calculated solids and residual melts are consistent with those registered in the San Gabriel pluton. The exception is the Na_2O trend that shows a peak close to 60 wt% SiO_2 (Figs. 6 and 11A). The composition of the samples lies in the tie-lines between the compositions of cumulate solids and the corresponding interstitial melt composition at different crystallinity stages (Fig. 11A; see Supplemental Material). However, we focus on the Na_2O content, which allows us to better constrain the composition of the interstitial melt and cumulate solids to reproduce the compositions recorded in the San Gabriel pluton because of the inflection observed in the concentrations.

Zr, Rb, and Sr Partitioning between Solid and Melt Phases

Simulations of Rb and Sr distribution between melt and solid phases during fractionation (Fig. 9B) indicate that the patterns observed in most of the San Gabriel pluton samples represent different mixing proportions between cumulate solids and extracted melt equivalent to the composition of the Los Piques quartz-monzonite. According to our simulations, the Rb/Sr ratio in the cumulate tends to decrease as the extracted melt fraction increases because of the compatibility behavior of Sr. Our results indicate that extraction of up to ~50 vol% of interstitial melts is necessary to reproduce San Gabriel pluton compositions (Fig. 9D).

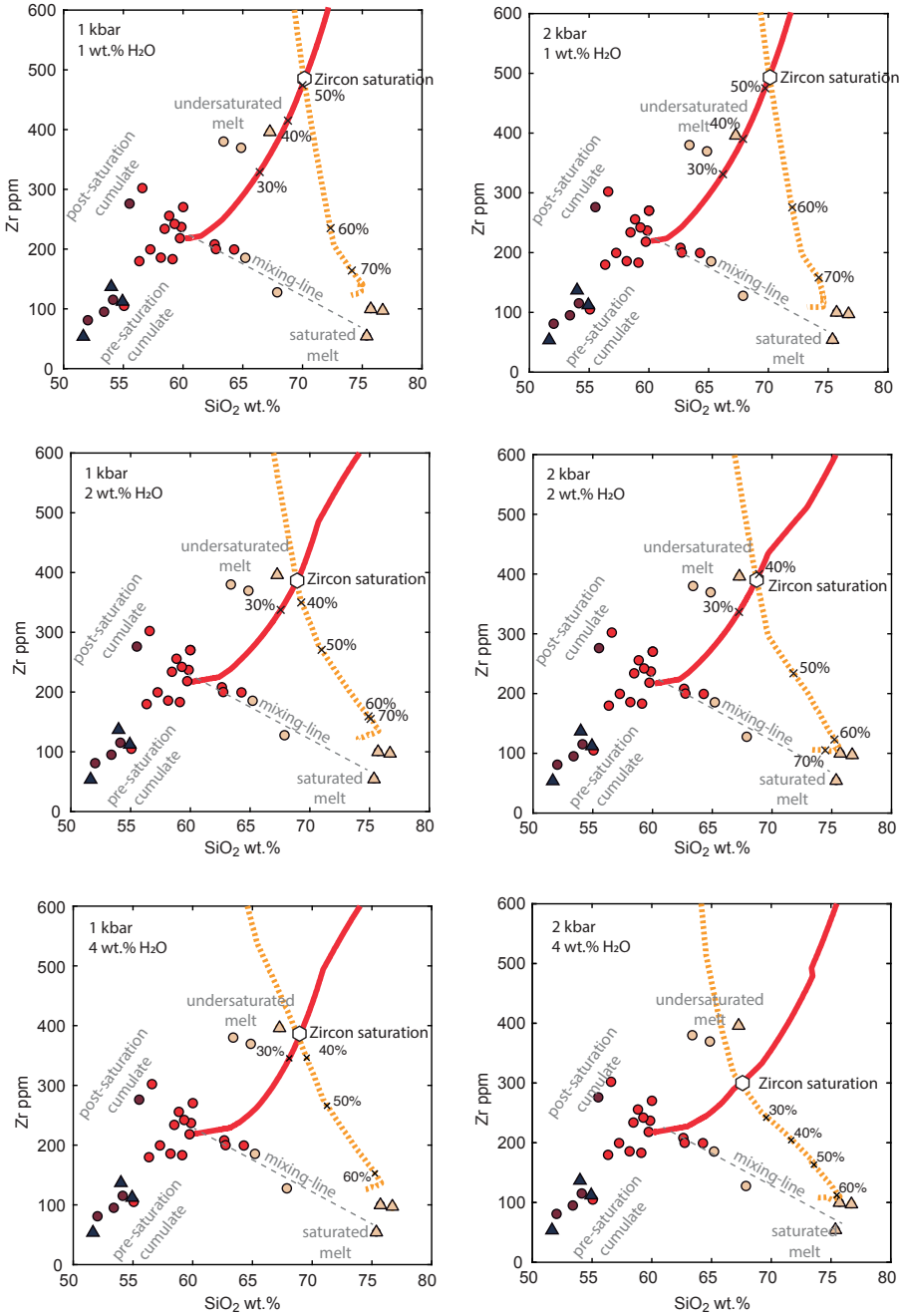

Figure 10. Plots show Zr concentration in the modeled liquid line of descent (red line), considering a parental magma with intermediate composition, equivalent to sample SG0702 (quartz-monzonite), and Zr concentration required for zircon saturation of the simulated melts at each composition (orange dotted line). Zr content in the residual melts was calculated assuming a perfect incompatibility, according to the formulation of Lee and Bachmann (2014). The zircon saturation curve was calculated according to the formulation of Watson et al. (2006). Magma crystallinity appears as percentages along the melt composition curves.

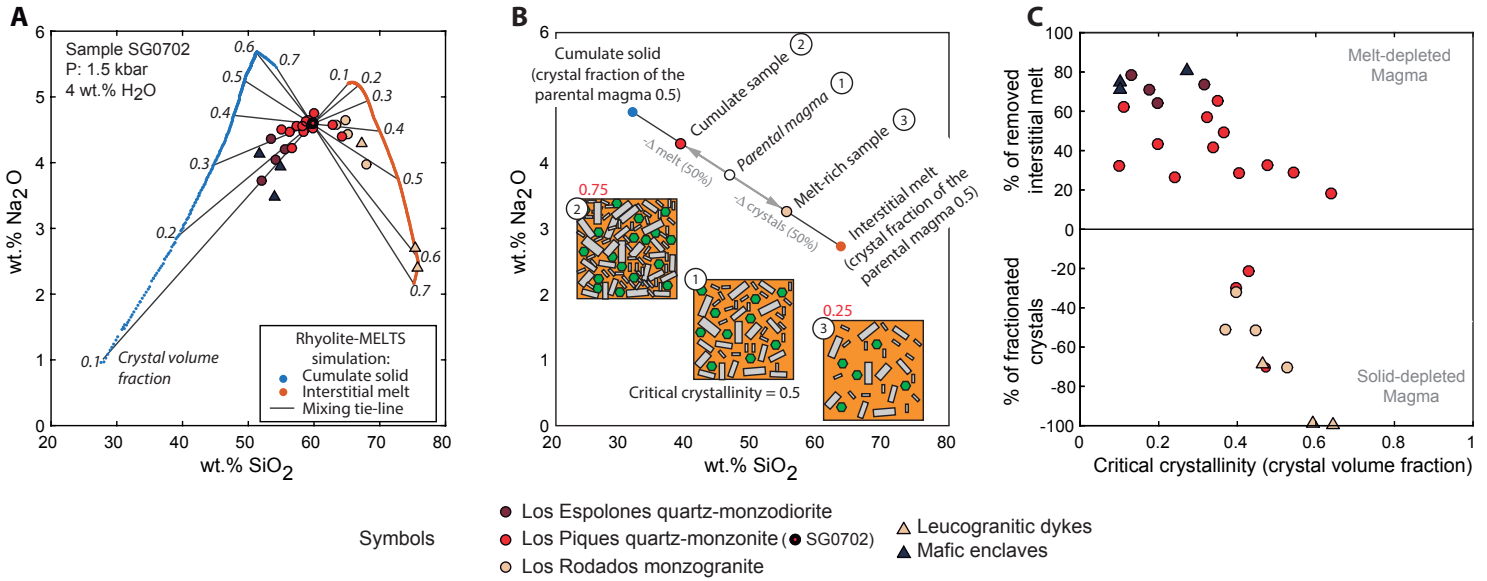

Figure 11. (A) Simulation plots Na_2O content in cumulate solid and interstitial melt (in equilibrium), and composition of the mixing of those phases in different amounts (gray lines), during the crystallization of a magma that has the bulk composition of the intermediate samples of the San Gabriel pluton (SG0702). Results were obtained through thermodynamic simulations by using Rhyolite-MELTS (Gualda et al., 2012). Numbers in italics show diverse crystal volume fractions of the parental magma and the cumulate solid and interstitial melt in equilibrium. (B) Scheme of the mass balance carried out to calculate the amount of interstitial melts removed from cumulate samples, or the amount of fractionated crystals in melt-rich samples. Critical crystallinity was calculated as the crystal volume fraction reached when the composition of the interstitial melt and residual solids reproduce the composition of each single sample, minimizing the sum of the least squares. Sketches show the appearance of the magma after (2) crystal accumulation and (3) crystal fractionation from (1) parental magma. (C) Amount of interstitial silicic melt extracted (positive values indicate melt-depleted magmas) or amount of fractionated crystals (negative values indicate crystal-depleted magmas) once the parent magma reached critical crystallinity and the crystal-melt separation occurred. Values were obtained via mass-balance calculations.

The composition of the Los Rodados monzogranites and leucogranitic dikes can also be reproduced by even higher amounts of extracted interstitial melts (up to 80 vol%) mixed with inherited crystals.

Zr saturation modeling results support the crystal-melt separation from an intermediate magma to explain the compositional variability of the San Gabriel pluton. Simulations show that the quartz-monzodiorites may be reproduced as cumulates that are generated after extraction of zircon undersaturated residual melts and before a 50% crystallinity is reached (Fig. 10). Some zircon-saturated melts could be trapped in the interstices, though, explaining the zircon occurrence in quartz-monzodiorites. The Zr-rich felsic monzogranites and leucocratic dike would represent Zr-undersaturated melts that were extracted from the parental magma. On the other hand, the Zr-poor monzogranites and some quartz-monzonites would correspond to different proportions of residual melts, extracted after zircon saturation, with between 50% and 70% crystals (even 40% of 2 kbar and 4 wt% H_2O; Fig. 10). Leucogranitic dikes represent late segregated melts that formed when the magma had a crystallinity of 70%.

Mass Balance and Determination of the Amount of Removed Residual Melts

The compositions of the San Gabriel pluton coincide with the mixing lines between the solid-melt pairs in equilibrium at different crystallinity states of the parental magma (Fig. 11A). A mass balance was carried out to calculate the volume fractions of removed melts or fractionated crystals from parental magma to reproduce each sample composition. This analysis assumes that the crystallizing magma contains solids and residual melts in equilibrium, which are almost instantly separated (partially or totally) at a certain crystallinity value (Dufek and Bachmann, 2010; Bachmann and Huber, 2019).

The procedure for each sample composition starts with determining the solids-melt pair whose mixing line can be used to reproduce the composition, minimizing the sum of the least squares of the major element concentrations of each single sample with the tie-line (Fig. 11B). The crystallinity of the initial magma when the sample compositions are reached is denoted as "critical crystallinity," which represents the crystal fraction of the parental magma when the crystal-melt separation occurs (Fig. 11B). Once critical crystallinity is determined, a

mass balance is carried out to calculate the volume fraction of removed residual melt (in the case of melt-depleted samples that represent cumulates) or the volume fraction of fractionated crystals (in case of compositions associated with the accumulation of residual melts).

Calculation of critical crystallinities indicates that: (1) the Los Espolones quartz-monzodiorites represent crystal-rich magmas that were generated by extracting between 60% and 80% of the total volume of haplogranitic residual melts (>67 wt% SiO_2) when the magma reached crystallinities of between 10% and 40%, resulting in a strong-cumulate signature (Fig. 11C); (2) the Los Piques quartz-monzonites would represent cumulates with lesser amounts of extracted interstitial melts (<50%) and formed in a wide spectrum of critical crystallinity (Fig. 11C); (3) the Los Rodados monzogranite represents residual melts (crystal-depleted) derived from extraction of the 30–70% of the available volume of melts from a mush with crystallinities of 40–55%; (4) leucogranitic dikes represent the totality of the melt extracted from a mush with 60% of crystallinity (Fig. 11C).

DISCUSSION

Crystal Residues and Interstitial Melts Segregation from Intermediate Magmas in Upper Crustal Plutons

Geochemical trends in Harker diagrams indicate that the magmatic units of the San Gabriel pluton were generated via fractionation processes. For instance, Sc content indicates the accumulation of amphibole, pyroxene, and magnetite, consistent with the higher MgO contents and modal abundance of these minerals in the Los Espolones quartz-monzodiorites (Fig. 7). The decreasing Sr content and increasing Rb content suggest plagioclase fractionation. However, the general increase in Ba and K_2O suggests that K-feldspar and biotite are late-crystallizing minerals (except in two leucogranitic dikes) that crystallized in late silicic melts. Some trace elements, such as Y, La, and Zr exhibit an increasing pattern as SiO_2 content increases up to 60 wt%. On the contrary, in samples with >60 wt% SiO_2, these elements' concentrations decrease, except for two monzogranite samples and one leucogranitic dike (Fig. 7). This pattern represents the well-known inflection due to zircon saturation.

The coarse-grained texture and polygonal crystal shapes observed in the quartz-monzonites, together with the decreased abundance of euhedral crystals compared to quartz-monzodiorites, suggest that those samples record the most representative composition of the parental magma where phases crystallized in equilibrium with limited segregation. Those features, together with the geochemical pattern exhibited by Rb and Sr concentrations, support the consideration of the sample SG0702 (~60 wt% of SiO_2) as a potential parental magma. Magma diversification from an intermediate composition has been proposed for other well-studied intrusives such as the Searchlight pluton (Nevada, USA; Gelman et al., 2014; Eddy et al., 2022), and La Gloria pluton (Mahood and Cornejo, 1992; Gutiérrez et al., 2013; Aravena et al., 2017) and Huemul-Risco Bayo pluton, both of which are in central Chile (Schaen et al., 2017; Garibaldi et al., 2018).

Despite all of the key information that such trace element models can provide, such modeling must be interpreted with caution, and considering some limitations. Using Rb and Sr to analyze their partition between solids and melts in a crystallizing magma is useful when plagioclase is the major fractionating phase as indicated by major element concentrations and the mineralogical record. Gelman et al. (2014) show that variable partition coefficients throughout the magma crystallization require that ratios of extracted melt and the crystallinity window of extraction must be carefully chosen, because Sr becomes compatible once plagioclase and K-feldspar crystallize, generating differences in the melt signatures if they are extracted before or during/after the crystallization of those phases (but showing cryptic differences in the cumulate signatures). In the case of the San Gabriel pluton, we chose the peak of melt extraction after the crystallization of plagioclase and during the crystallization of K-feldspar around 60% of crystallinity (Fig. 9B). However, our results show that high amounts of interstitial melt had to be removed from the parental magma to reproduce the felsic compositions (consistent with our results of mass balance analysis of the major elements), whereas most of the samples represent cumulates, which implies that changes in the variables of the trace element partition modeling should have limited impact on the results (Gelman et al., 2014). In addition, another limitation of the formulation is that the Rb mobility, especially in the presence of volatiles, may alter the initial pattern of the rocks. However, the well-defined variation of Rb and Sr concentrations with respect to the SiO_2 content suggests little mobility of those elements during the evolution of the San Gabriel pluton (Fig. 7).

Recognizing the parental magma composition in felsic intrusions through the whole-rock compositions has limitations, since the original composition can be obscured by the trapped residual melts within intermediate-silicic cumulates. The magma evolution in plutonic rocks usually deviates from the liquid descendent line, adding to the possibility that multiple liquid lines of descent can take place in a single magma reservoir (Barnes et al., 2016; Gelman et al., 2014). However, in this case, we show that first-order variations of San Gabriel pluton compositions can be generated from an intermediate parental magma that is equivalent to the quartz-monzonite because: (1) in general, the trace element patterns show an inflection point near that composition, suggesting the initiation of significant fractionation, and (2) textures indicate that the quartz-monzonite crystallized almost in equilibrium and without cumulate textures. This is also supported by numerical simulations of the Rb and Sr partition between the interstitial melt and cumulate phases. We carried out models that consider the composition of the parental magma equivalent to the sample SG2310, which corresponds to a quartz-monzodiorite of clinopyroxene and biotite collected from a mafic layer from the Los Espolones unit (Figs. 3E and 4A), with the same physical conditions as models with sample SG0702 (H_2O content, pressure, and fO_2 buffer). Results show that the extracted interstitial melts from mafic magma crystallization have compositions that differ from the compositions recorded in the San Gabriel pluton. The simulated melts are clearly depleted in Rb

compared to the quartz-monzonites and monzogranites (Fig. 9D), which supports that the mafic samples of the San Gabriel pluton do not represent late injections of mafic magma but instead are crystalline cumulates that formed after the removal of interstitial silicic melts.

The models of crystal-melt separation in magma reservoirs invoke a specific crystallinity window where the segregation occurs, which is typically associated with the rheological locking of the magma between 50% and 70% (Dufek and Bachmann, 2010). Some experimental studies also propose that the rheological locking of plagioclase-bearing magma reaches around 30–50% of crystal content because of the crystals' elongate shape (summary in Bachmann and Huber, 2019). The optimal crystallinity for melt extraction value also depends on the physical mechanism that controls the crystal-melt separation, such as compaction of the crystalline mush yield by gravitational collapse, crystal repacking, porous media transport, or channelization along dike-like structures. The physical mechanism of crystal-melt separation is out of the scope of this study; however, it is interesting to note that the critical crystallinities obtained from the mass balance are between 0.15 and 0.6 in crystal volume fractions, with the highest amounts of removed melts between 0.3 and 0.6 (Fig. 11C), which is consistent with other studies. It is also interesting to note that a critical crystallinity of 60%, similar to the optimal crystallinity value proposed by Dufek and Bachmann (2010), is needed to explain the leucogranitic dike melt segregation.

Magmatic Evolution of the San Gabriel Pluton: From the Field and Compositional Observations

Based on field and geochemical evidence presented here, we interpret that the San Gabriel pluton represents a magma reservoir where significant magma differentiation took place at the emplacement level accompanied by silicic melt redistribution into the reservoir during the formation of the Los Rodados monzogranite (Fig. 12). The textural and compositional variability in the San Gabriel pluton could be interpreted as in situ crystallization and subsequent mass redistribution giving rise to cumulate compositional signatures and the observed magmatic structures, which are preserved because of limited compositional homogenization of the reservoir after magma differentiation.

Field evidence, such as the contact relationships, allows us to infer a relative temporal succession of events during San Gabriel pluton assembly. These events are grouped in two stages (Fig. 12). Because of the overlapping ages and the lack of sharp internal contacts in the Los Piques quartz-monzonites (the main intrusive rocks hosting the rest of the units), we suggest this unit was constructed forming a homogeneous reservoir with composition equivalent to that of the parental magma (~60 wt%

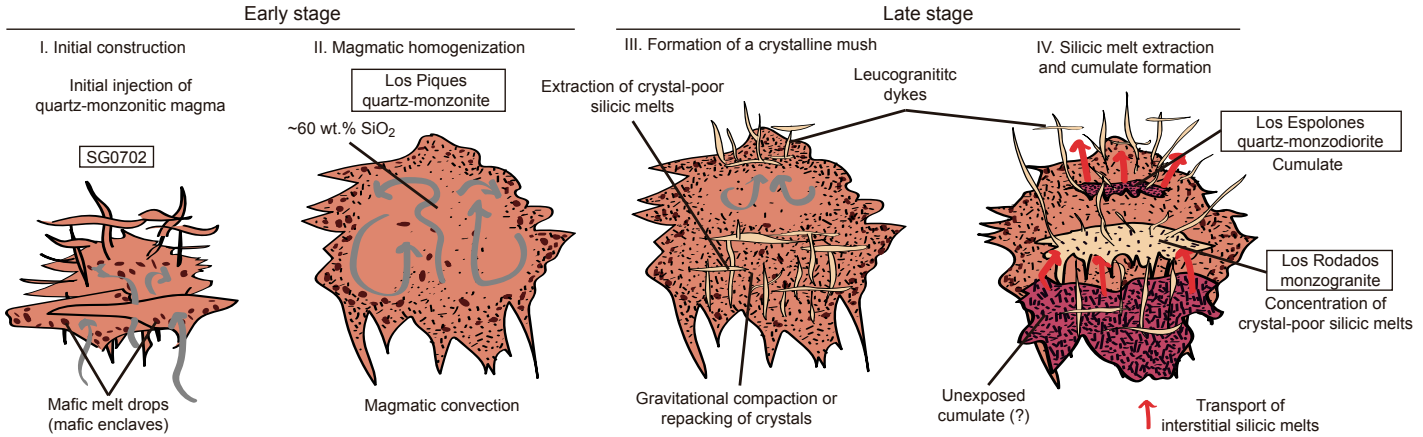

Figure 12. Conceptual model proposed for San Gabriel pluton construction is shown (lighter colors represent more silicic compositions, according to the symbology of previous figures). I. Early pluton construction stage via initial injections of magma with intermediate composition with mafic melt drops (mafic enclaves). II. Homogenization and stirring, where the magma reservoir is built with probable whole-scale convection, homogenization, and poor residual melt extraction (Los Piques quartz-monzonite). Mafic enclaves were predominantly preserved in the reservoir's borders. III. Formation of a mushy reservoir with intermediate crystallinities, decreasing the magmatic convection and favoring the occurrence of crystal-melt separation. Interstitial silicic melts were probably extracted because of the gravitational mush compaction or crystal repacking. Silicic melts formed tabular channels that migrate upward because of the lower density than that of the crystalline mush. IV. Final San Gabriel pluton assemblage, where concentration of crystal-poor silicic melts generated the Los Rodados monzogranites as a silicic cap. A crystal-rich cumulate zone was probably formed in lower, unexposed pluton levels. Almost simultaneously, in the upper part of the reservoir, melt extraction gave rise to the cumulate Los Espolones quartz-monzodiorite. Residual melts were transported upward and accumulated as leucogranitic dikes preserved in the upper part of the pluton and host rocks.

SiO_2; early stage in Fig. 12) and representing the oldest rocks, similar to the proposed magmatic evolution in other intrusives like the Spirit Mountain pluton (Walker et al., 2007). Because the mafic enclaves are mainly preserved in the pluton borders, they should be part of the initial injections as immiscible melts with the parental magma, representing mafic melt drops within the convective felsic magma (see Barbarin, 2005).

In a later stage, when magmatic convection started to slow down in response to the high crystal content of the magma, crystal-melt separation occurred as melt extraction in mushes at intermediate crystallinities (likely via gravitational compaction or crystal repacking; see Bachmann and Huber, 2019, and references therein). This scenario allowed the generation of the cumulate Los Espolones quartz-monzodiorites (representing melt-depleted magmas) and the generation of the Los Rodados monzogranites (representing extracted and redistributed silicic melts that intruded the hosting Los Piques quartz-monzonites, which was in solid-state; late stage in Fig. 12). We interpret that cumulate formation and silicic melt canalization started to occur roughly contemporaneously with the last convective flows in the core of the reservoir, which explains the presence of some enclaves from the Los Espolones quartz-monzodiorite contained in Los Piques quartz-monzonites (Fig. 4A). We rule out the idea that the Los Rodados monzogranites were extracted directly from the Los Espolones quartz-monzodiorites, because the relatively low density of the silicic melts would favor an upward transport, hindering the feeding of the felsic unit located in the lower parts of the pluton. This could be understood if the Los Rodados monzogranites had been formed by the amalgamation of residual melts extracted and transported upward from deeper levels of the San Gabriel pluton reservoir, probably leaving behind an unexposed mafic cumulate zone (Fig. 12). Almost simultaneously (according to the overlapping ages), the Los Espolones quartz-monzodiorites were generated, which are testimonies to a cumulate counterpart of upward-extracted residual melts recorded as leucogranitic dikes preserved in the roof of the pluton, which formed during late stages.

The U-Pb dates in zircon suggest that the San Gabriel pluton has a longevity of ca. 1.1 Ma, with the youngest and oldest ages being 12.41 ± 0.08 Ma and 13.57 ± 0.08 Ma, respectively (Fig. 8 and Table S3, see footnote 1). Most of the samples present cooling ages that overlap the weighted San Gabriel pluton mean, though, with no significant differences between the three magmatic units. This implies that the interval time for the crystal-melt separation and the late intrusion of the monzogranite assembly lasted up to 500 k.y. (from the error span of the dating method), which indicates that the San Gabriel pluton was constructed through short-lived magma pulses. This scenario is also supported by the sharp contacts between the different magmatic domains of the pluton (Fig. 4). In this sense, we emphasize that higher-precision U-Pb zircon methods should be applied to better quantify the timespan between the initial emplacement and the different events of late silicic melt-rich magma redistribution to generate the quartz-monzodiorites and monzogranites.

In the model we propose here, each unit is reproduced by the combination of the compositions of the interstitial melt and solid phases in equilibrium from a single crystallization sequence. We reiterate that the proposed model does not imply that each unit is the counterpart of another due to a unique differentiation event (for instance, Los Piques monzogranites could have been extracted from a deeper level and leave a residue analogous to Los Espolones quartz-monzodiorite). However, given the rheological rigidity resulting from the high mineral load required to generate some units, the overlap of cooling ages, and the magmatic interaction contacts between units, we emphasize that the differentiation processes must have occurred mainly within the reservoir.

Upper crustal intermediate-felsic magma reservoirs are considered to be potential sources of rhyolitic magmas that feed explosive eruptions, connecting silicic volcanism with granitic intrusions (Smith, 1960; Hildreth, 1981; Lipman, 1984; Metcalf, 2004; Bachmann et al., 2007; Schaen et al., 2017; Tavazzani et al., 2020; Du et al., 2022). This has been proposed, for example, in volcanic systems with large magma reservoirs (Druitt and Bacon, 1989; Brown et al., 1998; de Silva et al., 2006; Hildreth and Wilson, 2007; Deering et al., 2011b; Folkes et al., 2011; Lipman and Bachmann, 2015). Although magmatic differentiation via crystal-melt separation in the upper crustal levels may represent a significant process to generate dacitic to rhyolitic volcanism (Vazquez and Reid, 2002; Clemens, 2003; Deering et al., 2011a; Lee and Morton, 2015; Bachmann and Huber, 2019; Cornet et al., 2022), in the case of the San Gabriel pluton, concentration and an upward transportation of residual magma able to supply more than 500 km^3 of vigorous felsic eruptions is not likely. This is supported by the nearly eutectic and H_2O-saturated crystallization (evidenced by the presence of miarolitic cavities) of the high-silica magma and the fact that, according to the mass balance presented in this work, a higher volume of cumulates should be preserved in the pluton (which is difficult considering that the San Gabriel pluton has only 40 km^2 of areal exposure). The inability to supply rhyolitic volcanic eruptions was also proposed from numerical simulations and field data for the La Gloria pluton (Aravena et al., 2017), an intrusion that is spatiotemporally related to the San Gabriel pluton. The volume of silicic magma removed could be quantified by determining the volume of preserved cumulates in the reservoir in the San Gabriel pluton (which is made difficult by the limited exposition of the Los Espolones quartz-monzodiorite and is outside of the scope of this study), because the silicic melt record is incomplete due to the erosion. However, leucocratic dikes and breccias preserved within the host rock indicate that some felsic material removed was advected out of the reservoir.

CONCLUSIONS

Through a combination of field observations, petrography, whole-rock geochemistry, U-Pb zircon geochronology, and geochemical modeling, this study documents the San Gabriel pluton, a composite upper crustal intrusive that represents the final product of the evolution of a single magma reservoir. The pluton is composed of three magmatic units with a wide compositional spectrum (52–75 wt% SiO_2), and quartz-monzonites that host quartz-monzodiorites with cumulate textures are

disposed in the middle part of the pluton, and monzogranites are preserved in the lower part.

Geochemical data and geochemical modeling of trace element partitioning between solid phases and interstitial silicic melts suggest that the reservoir underwent magma differentiation via crystal-melt separation at the emplacement level from intermediate magmas equivalent to the quartz-monzonites. The mass balance of major element concentrations indicates that quartz-monzodiorites represent accumulated melt-depleted magmas after 50–80% of the available haplogranitic interstitial melts were extracted. On the other hand, the felsic rocks that form part of the monzogranites and leucogranitic dikes represent remobilized silicic melts that were concentrated in the lower exposure level of the pluton, which were transported upward from lower parts of the reservoir formed by the early crystallized magmas. Mass-balance results suggest that those melts were extracted when the intermediate magma had crystallinities of between 40% and 55%. According to U-Pb zircon geochronology, the magma reservoir had a lifetime of ca. 1.1 Ma and showed almost coeval crystallization of the whole system (since sample ages overlap the global weighted mean).

This study illustrates that the mechanism of crystal-melt separation from magmas with intermediate composition may explain the compositional variability in composite plutons and advocates for the role of upper crustal magma reservoirs in generating dacitic and rhyolitic magmas.

ACKNOWLEDGMENTS

This research was developed by the Chilean National Commission for Science and Technology (CONICYT) projects (FONDECYT #1180577 and REDES #150063) and the Fund for Publication Developments project (PEP I-2019071) granted by Universidad Mayor-Vicerrectoría de Investigación. I. Payacán was supported by the CONICYT doctoral grant (PFCHA-CONICYT #21151102). O. Bachmann was supported by the Swiss National Science Foundation (grant #200021_155923). We thank Lorenzo Tavazzani for his friendly and helpful review and valuable comments on this manuscript.

REFERENCES CITED

Aravena, A., Gutiérrez, F.J., Parada, M.A., Payacán, Í., Bachmann, O., and Poblete, F., 2017, Compositional zonation of the shallow La Gloria pluton (Central Chile) by late-stage extraction/redistribution of residual melts by channelization: Numerical modeling: Lithos, v. 284–285, p. 578–587, https://doi.org/10.1016/j.lithos.2017.05.013.

Bachl, C.A., Miller, C.F., Miller, J.S., and Faulds, J.E., 2001, Construction of a pluton: Evidence from an exposed cross section of the Searchlight pluton, Eldorado Mountains, Nevada: Geological Society of America Bulletin, v. 113, p. 1213–1228, https://doi.org/10.1130/0016-7606(2001)113<1213:COAPEF>2.0.CO;2.

Bachmann, O., and Bergantz, G.W., 2008, Rhyolites and their source mushes across tectonic settings: Journal of Petrology, v. 49, p. 2277–2285, https://doi.org/10.1093/petrology/egn068.

Bachmann, O., and Huber, C., 2016, Silicic magma reservoirs in the Earth's crust: The American Mineralogist, v. 101, p. 2377–2404, https://doi.org/10.2138/am-2016-5675.

Bachmann, O., and Huber, C., 2019, The inner workings of crustal distillation columns; the physical mechanisms and rates controlling phase separation in silicic magma reservoirs: Journal of Petrology, v. 60, p. 3–18, https://doi.org/10.1093/petrology/egy103.

Bachmann, O., Miller, C.F., and de Silva, S.L., 2007, The volcanic-plutonic connection as a stage for understanding crustal magmatism: Journal of Volcanology and Geothermal Research, v. 167, p. 1–23, https://doi.org/10.1016/j.jvolgeores.2007.08.002.

Barbarin, B., 2005, Mafic magmatic enclaves and mafic rocks associated with some granitoids of the central Sierra Nevada batholith, California: Nature, origin, and relations with the hosts: Lithos, v. 80, p. 155–177, https://doi.org/10.1016/j.lithos.2004.05.010.

Barnes, C.G., Coint, N., and Yoshinobu, A., 2016, Crystal accumulation in a tilted arc batholith: The American Mineralogist, v. 101, p. 1719–1734, https://doi.org/10.2138/am-2016-5404.

Barnes, C.G., Werts, K., Memeti, V., and Ardill, K., 2019, Most granitoid rocks are cumulates: Deductions from hornblende compositions and zircon saturation: Journal of Petrology, v. 60, p. 2227–2240, https://doi.org/10.1093/petrology/egaa008.

Bergantz, G.W., 2000, On the dynamics of magma mixing by reintrusion: Implications for pluton assembly processes: Journal of Structural Geology, v. 22, p. 1297–1309, https://doi.org/10.1016/S0191-8141(00)00053-5.

Brahm, R., Parada, M.A., Morgado, E., Contreras, C., and McGee, L.E., 2018, Origin of Holocene trachyte lavas of the Quetrupillán volcanic complex, Chile: Examples of residual melts in a rejuvenated crystalline mush reservoir: Journal of Volcanology and Geothermal Research, v. 357, p. 163–176, https://doi.org/10.1016/j.jvolgeores.2018.04.020.

Brown, S.J.A., Wilson, C.J.N., Cole, J.W., and Wooden, J., 1998, The Whakamaru group ignimbrites, Taupo Volcanic Zone, New Zealand: Evidence for reverse tapping of a zoned silicic magmatic system: Journal of Volcanology and Geothermal Research, v. 84, p. 1–37, https://doi.org/10.1016/S0377-0273(98)00020-1.

Cashman, K.V., Sparks, R.S.J., and Blundy, J.D., 2017, Vertically extensive and unstable magmatic systems: A unified view of igneous processes: Science, v. 355, https://doi.org/10.1126/science.aag3055.

Charrier, R., Baeza, O., Elgueta, S., Flynn, J.J., Gans, P., Kay, S.M., Muñoz, N., Wyss, A.R., and Zurita, E., 2002, Evidence for Cenozoic extensional basin development and tectonic inversion south of the flat-slab segment, southern Central Andes, Chile (33°–36°S.L.): Journal of South American Earth Sciences, v. 15, p. 117–139, https://doi.org/doi.org/10.1016/S0895-9811(02)00009-3.

Clemens, J.D., 2003, S-type granitic magmas—petrogenetic issues, models and evidence: Earth-Science Reviews, v. 61, p. 1–18, https://doi.org/10.1016/S0012-8252(02)00107-1.

Coleman, D.S., Gray, W., and Glazner, A.F., 2004, Rethinking the emplacement and evolution of zoned plutons: Geochronologic evidence for incremental assembly of the Tuolumne Intrusive Suite, California: Geology, v. 32, p. 433–436, https://doi.org/10.1130/G20220.1.

Coleman, D.S., Bartley, J.M., Glazner, A.F., and Pardue, M.J., 2012, Is chemical zonation in plutonic rocks driven by changes in source magma composition or shallow-crustal differentiation?: Geosphere, v. 8, p. 1568–1587, https://doi.org/10.1130/GES00798.1.

Cornejo, P.C., and Mahood, G.A., 1997, Seeing past the effects of re-equilibration to reconstruct magmatic gradients in plutons: La Gloria Pluton, central Chilean Andes: Contributions to Mineralogy and Petrology, v. 127, p. 159–175, https://doi.org/10.1007/s004100050273.

Cornet, J., Bachmann, O., Ganne, J., Fiedrich, A., Huber, C., Deering, C.D., and Feng, X., 2022, Assessing the effect of melt extraction from mushy reservoirs on compositions of granitoids: From a global database to a single batholith: Geosphere, v. 18, p. 985–999, https://doi.org/10.1130/GES02333.1.

de Silva, S.L., and Gregg, P.M., 2014, Thermomechanical feedbacks in magmatic systems: Implications for growth, longevity, and evolution of large caldera-forming magma reservoirs and their supereruptions: Journal of Volcanology and Geothermal Research, v. 282, p. 77–91, https://doi.org/10.1016/j.jvolgeores.2014.06.001.

de Silva, S., Zandt, G., Trumbull, R., Viramonte, J.G., Salas, G., and Jiménez, N., 2006, Large ignimbrite eruptions and volcano-tectonic depressions in the Central Andes: A thermomechanical perspective, *in* Troise, C., De Natale, G., and Kilburn, C.J.R., eds., Mechanisms of Activity and Unrest at Large Calderas: Geological Society, London, Special Publication 269, p. 47–63, https://doi.org/10.1144/GSL.SP.2006.269.01.04.

Deckart, K., Godoy, E., Bertens, A., Jerez, D., and Saeed, A., 2010, Barren Miocene granitoids in the Central Andean metallogenic belt, Chile: Geochemistry and Nd-Hf and U-Pb isotope systematics: Andean Geology, v. 37, p. 1–31, https://doi.org/10.4067/S0718-71062010000100001.

Deering, C.D., and Bachmann, O., 2010, Trace element indicators of crystal accumulation in silicic igneous rocks: Earth and Planetary Science Letters, v. 297, p. 324–331, https://doi.org/10.1016/j.epsl.2010.06.034.

Deering, C.D., Bachmann, O., and Vogel, T.A., 2011a, The Ammonia Tanks Tuff: Erupting a melt-rich rhyolite cap and its remobilized crystal cumulate: Earth and Planetary Science Letters, v. 310, p. 518–525, https://doi.org/10.1016/j.epsl.2011.08.032.

Deering, C.D., Cole, J.W., and Vogel, T.A., 2011b, Extraction of crystal-poor rhyolite from a hornblende-bearing intermediate mush: A case study of the caldera-forming Matahina eruption, Okataina volcanic complex: Contributions to Mineralogy and Petrology, v. 161, p. 129–151, https://doi.org/10.1007/s00410-010-0524-0.

Druitt, T.H., and Bacon, C.R., 1989, Petrology of the zoned calc-alkaline magma chamber of Mount Mazama, Crater Lake, Oregon: Contributions to Mineralogy and Petrology, v. 101, p. 245–259, https://doi.org/10.1007/BF00375310.

Du, D.-H., Wang, X.-L., Wang, S., Miller, C.F., Xu, X., Chen, X., and Zhang, F.-F., 2022, Deciphering cryptic multi-stage crystal-melt separation during construction of the Tonglu Volcanic–Plutonic Complex, SE China: Journal of Petrology, v. 63, https://doi.org/10.1093/petrology/egab098.

Dufek, J., and Bachmann, O., 2010, Quantum magmatism: Magmatic compositional gaps generated by melt-crystal dynamics: Geology, v. 38, p. 687–690, https://doi.org/10.1130/G30831.1.

Eddy, M.P., Pamukçu, A., Schoene, B., Steiner-Leach, T., and Bell, E.A., 2022, Constraints on the timescales and processes that led to high-SiO_2 rhyolite production in the Searchlight pluton, Nevada, USA: Geosphere, v. 18, p. 1000–1019, https://doi.org/10.1130/GES02439.1.

Farías, M., Charrier, R., Carretier, S., Martinod, J., Fock, A., Campbell, D., Cáceres, J., and Comte, D., 2008, Late Miocene high and rapid surface uplift and its erosional response in the Andes of central Chile (33°–35°S): Tectonics, v. 27, https://doi.org/10.1029/2006TC002046.

Farina, F., Dini, A., Innocenti, F., Rocchi, S., and Westerman, D.S., 2010, Rapid incremental assembly of the Monte Capanne pluton (Elba Island, Tuscany) by downward stacking of magma sheets: Geological Society of America Bulletin, v. 122, p. 1463–1479, https://doi.org/10.1130/B30112.1.

Fiedrich, A.M., Bachmann, O., Ulmer, P., Deering, C.D., Kunze, K., and Leuthold, J., 2017, Mineralogical, geochemical, and textural indicators of crystal accumulation in the Adamello Batholith (Northern Italy): The American Mineralogist, v. 102, p. 2467–2483, https://doi.org/10.2138/am-2017-6026.

Fock, A., 2005, Cronología y Tectónica de la exhumación en el Neógeno de los Andes de Chile Central entre los 33° y los 34° S [M.Sc. thesis]: Santiago, Universidad de Chile, 179 p.

Folkes, C.B., De Silva, S.L., Schmitt, A.K., and Cas, R.A.F., 2011, A reconnaissance of U-Pb zircon ages in the Cerro Galán system, NW Argentina: Prolonged magma residence, crystal recycling, and crustal assimilation: Journal of Volcanology and Geothermal Research, v. 206, p. 136–147, https://doi.org/10.1016/j.jvolgeores.2011.06.001.

Frazer, R.S., Coleman, D.S., and Mills, R.D., 2014, Zircon U-Pb geochronology of the Mount Givens Granodiorite: Implications for the genesis of large volumes of eruptible magma: Journal of Geophysical Research: Solid Earth, v. 119, p. 2907–2924, https://doi.org/10.1002/2013JB010716.

Garibaldi, N., Tikoff, B., Schaen, A.J., and Singer, B.S., 2018, Interpreting granitic fabrics in terms of rhyolitic melt segregation, accumulation, and escape via tectonic filter pressing in the Huemul Pluton, Chile: Journal of Geophysical Research: Solid Earth, v. 123, p. 8548–8567, https://doi.org/10.1029/2018JB016282.

Gelman, S.E., Deering, C.D., Bachmann, O., Huber, C., and Gutiérrez, F.J., 2014, Identifying the crystal graveyards remaining after large silicic eruptions: Earth and Planetary Science Letters, v. 403, p. 299–306, https://doi.org/10.1016/j.epsl.2014.07.005.

Glazner, A., Bartley, J., Coleman, D.S., Gray, W., and Taylor, R.Z., 2004, Are plutons assembled over millions of years by amalgamation from small magma chambers?: GSA Today, v. 14, no. 4–5, p. 4–11, https://doi.org/10.1130/1052-5173(2004)014<0004:APAOMO>2.0.CO;2.

Gray, W., Glazner, A.F., Coleman, D.S., and Bartley, J.M., 2008, Long-term geochemical variability of the Late Cretaceous Tuolumne Intrusive Suite, central Sierra Nevada, California, *in* Annen, C., and Zellmer, G.F., eds., Dynamics of Crustal Magma Transfer, Storage and Differentiation: Geological Society, London, Special Publication 304, p. 183–201, https://doi.org/10.1144/SP304.10.

Gualda, G.A.R., Ghiorso, M.S., Lemons, R.V., and Carley, T.L., 2012, Rhyolite-MELTS: A modified calibration of MELTS optimized for silica-rich, fluid-bearing magmatic systems: Journal of Petrology, v. 53, p. 875–890, https://doi.org/10.1093/petrology/egr080.

Guillong, M., Meier, D.L., Allan, M.M., Heinrich, C.A., and Yardley, B.W.D., 2008, Appendix A6: SILLS: A MATLAB-based program for the reduction of laser-ablation ICP-MS data of homogeneous materials and inclusions: Mineralogical Association of Canada Short Course, v. 40, p. 328–333.

Guillong, M., Sliwinski, J.T., Schmitt, A., Forni, F., and Bachmann, O., 2016, U-Th zircon dating by laser ablation single collector inductively coupled plasma-mass spectrometry (LA-ICP-MS): Geostandards and Geoanalytical Research, v. 40, p. 377–387, https://doi.org10.1111/j.1751-908X.2016.00396.x.

Gutiérrez, F., Payacán, Í., Gelman, S., Bachmann, O., and Parada, M.A., 2013, Late-stage magma flow in a shallow felsic reservoir: Merging the anisotropy of magnetic susceptibility record with numerical simulations in La Gloria Pluton, central Chile: Journal of Geophysical Research: Solid Earth, v. 118, p. 1984–1998, https://doi.org/10.1002/jgrb.50164.

Gutiérrez, F., Payacán, I., Szymanowski, D., Guillong, M., Bachmann, O., and Parada, M.A., 2018, Lateral magma propagation during the emplacement of La Gloria Pluton, central Chile: Geology, v. 46, p. 1051–1054, https://doi.org/10.1130/G45361.1.

Hartung, E., Caricchi, L., Floess, D., Wallis, S., Harayama, S., Kouzmanov, K., and Chiaradia, M., 2017, Evidence for residual melt extraction in the Takidani Pluton, Central Japan: Journal of Petrology, v. 58, p. 763–788, https://doi.org/10.1093/petrology/egx033.

Hawkins, D.P., and Wiebe, R.A., 2004, Discrete stoping events in granite plutons: A signature of eruptions from silicic magma chambers?: Geology, v. 32, p. 1021–1024, https://doi.org/10.1130/G21083.1.

Hildreth, W., 1981, Gradients in silicic magma chambers: Implications for lithospheric magmatism: Journal of Geophysical Research: Solid Earth, v. 86, p. 10,153–10,192, https://doi.org/10.1029/JB086iB11p10153.

Hildreth, W.E.S., and Wilson, C.J.N., 2007, Compositional zoning of the Bishop Tuff: Journal of Petrology, v. 48, p. 951–999, https://doi.org/10.1093/petrology/egm007.

Holness, M.B., 2018, Melt segregation from silicic crystal mushes: A critical appraisal of possible mechanisms and their microstructural record: Contributions to Mineralogy and Petrology, v. 173, p. 1–17, https://doi.org/10.1007/s00410-018-1465-2.

Jacob, K.H., Farmer, G.L., Buchwaldt, R., and Bowring, S.A., 2015, Deep crustal anatexis, magma mixing, and the generation of epizonal plutons in the Southern Rocky Mountains, Colorado: Contributions to Mineralogy and Petrology, v. 169, p. 1–23, https://doi.org/10.1007/s00410-014-1094-3.

Jellinek, A.M., and Kerr, R.C., 1999, Mixing and compositional stratification produced by natural convection 2. Applications to the differentiation of basaltic and silicic magma chambers and komatiite lava flows: Journal of Geophysical Research: Solid Earth, v. 104, p. 7203–7218, https://doi.org/10.1029/1998JB900117.

Karakas, O., Dufek, J., Mangan, M.T., Wright, H.M., and Bachmann, O., 2017, Thermal and petrologic constraints on lower crustal melt accumulation under the Salton Sea Geothermal Field: Earth and Planetary Science Letters, v. 467, p. 10–17, https://doi.org/10.1016/j.epsl.2017.02.027.

Laumonier, M., Scaillet, B., Pichavant, M., Champallier, R., Andujar, J., and Arbaret, L., 2014, On the conditions of magma mixing and its bearing on andesite production in the crust: Nature Communications, v. 5, p. 1–12, https://doi.org/10.1038/ncomms6607.

Kurtz, A.C., Kay, S.M., Charrier, R., and Farrar, E., 1997, Geochronology of Miocene plutons and exhumation history of the El Teniente region, Central Chile (34-35°8): Revista Geológica de Chile, v. 24, p. 75–90, https://doi.org/10.5027/andgeoV24n1-a05.

Lee, C.-T.A., and Bachmann, O., 2014, How important is the role of crystal fractionation in making intermediate magmas? Insights from Zr and P systematics: Earth and Planetary Science Letters, v. 393, p. 266–274, https://doi.org/10.1016/j.epsl.2014.02.044.

Lee, C.-T.A., and Morton, D.M., 2015, High silica granites: Terminal porosity and crystal settling in shallow magma chambers: Earth and Planetary Science Letters, v. 409, p. 23–31, https://doi.org/10.1016/j.epsl.2014.10.040.

Lee, C.-T.A., Morton, D.M., Farner, M.J., and Moitra, P., 2015, Field and model constraints on silicic melt segregation by compaction/hindered settling: The role of water and its effect on latent heat release: The American Mineralogist, v. 100, p. 1762–1777, https://doi.org/10.2138/am-2015-5121.

Leuthold, J., Müntener, O., Baumgartner, L.P., Putlitz, B., Ovtcharova, M., and Schaltegger, U., 2012, Time resolved construction of a bimodal laccolith (Torres del Paine, Patagonia): Earth and Planetary Science Letters, v. 325–326, p. 85–92, https://doi.org/10.1016/j.epsl.2012.01.032.

Lindsay, J.M., Schmitt, A.K., Trumbull, R.B., de Silva, S.L., Siebel, W., and Emmermann, R., 2001, Magmatic evolution of the La Pacana Caldera System, Central Andes, Chile: Compositional variation of two cogenetic, large-volume felsic ignimbrites: Journal of Petrology, v. 42, p. 459–486, https://doi.org/10.1093/petrology/42.3.459.

Lipman, P.W., 1984, The roots of ash flow calderas in western North America: Windows into the tops of granitic batholiths: Journal of Geophysical Research: Solid Earth, v. 89, p. 8801–8841, https://doi.org/10.1029/JB089iB10p08801.

Lipman, P.W., 2007, Incremental assembly and prolonged consolidation of Cordilleran magma chambers: Evidence from the Southern Rocky Mountain volcanic field: Geosphere, v. 3, p. 42–70, https://doi.org/10.1130/GES00061.1.

Lipman, P.W., and Bachmann, O., 2015, Ignimbrites to batholiths: Integrating perspectives from geological, geophysical, and geochronological data: Geosphere, v. 11, p. 705–743, https://doi.org/10.1130/GES01091.1.

Ludwig, K.R., 2008, User's Manual for Isoplot/Ex Version 3.70: A Geochronology Toolkit for Microsoft Excel: Berkeley Geochronological Center Special Publication 4, p. 1–76.

Mahood, G., 1990, Second reply to comment of R.S.J. Sparks, H.E. Huppert and C.J.N. Wilson on "Evidence for long residence times of rhyolitic magma in the Long Valley magmatic system: The isotopic record in the precaldera lavas of Glass Mountain": Earth and Planetary Science Letters, v. 99, p. 395–399, https://doi.org/10.1016/0012-821X(90)90145-N.

Mahood, G.A., and Cornejo, P.C., 1992, Evidence for ascent of differentiated liquids in a silicic magma chamber found in a granitic pluton: Earth and Environmental Science Transactions of the Royal Society of Edinburgh, v. 83, p. 63–69, https://doi.org/10.1017/S0263593300007756.

Marsh, B.D., 1989, Magma chambers: Annual Review of Earth and Planetary Sciences, v. 17, p. 439–474, https://doi.org/10.1146/annurev.ea.17.050189.002255.

Matzel, J.E.P., Bowring, S.A., and Miller, R.B., 2006, Time scales of pluton construction at differing crustal levels: Examples from the Mount Stuart and Tenpeak intrusions, North Cascades, Washington: Geological Society of America Bulletin, v. 118, p. 1412–1430, https://doi.org/10.1130/B25923.1.

McNulty, B.A., Tong, W., and Tobisch, O., 1996, Assembly of a dike-fed magma chamber: The Jackass Lakes pluton, central Sierra Nevada, California: Geological Society of America Bulletin, v. 108, no. 8, p. 926–940, https://doi.org/10.1130/0016-7606(1996)108<0926:AOADFM>2.3.CO;2.

Metcalf, R.V., 2004, Volcanic–plutonic links, plutons as magma chambers and crust–mantle interaction: A lithospheric scale view of magma systems: Earth and Environmental Science Transactions of the Royal Society of Edinburgh, v. 95, p. 357–374, https://doi.org/10.1017/S0263593300001127.

Michel, J., Baumgartner, L., Putlitz, B., Schaltegger, U., and Ovtcharova, M., 2008, Incremental growth of the Patagonian Torres del Paine laccolith over 90 k.y.: Geology, v. 36, p. 459–462, https://doi.org/10.1130/G24546A.1.

Middlemost, E.A.K., 1994, Naming materials in the magma/igneous rock system: Earth-Science Reviews, v. 37, p. 215–224, https://doi.org/10.1016/0012-8252(94)90029-9.

Miller, C.F., Furbish, D.J., Walker, B.A., Claiborne, L.L., Koteas, G.C., Bleick, H.A., and Miller, J.S., 2011, Growth of plutons by incremental emplacement of sheets in crystal-rich host: Evidence from Miocene intrusions of the Colorado River region, Nevada, USA: Tectonophysics, v. 500, p. 65–77, https://doi.org/10.1016/j.tecto.2009.07.011.

Miller, J.S., 2008, Assembling a pluton…one increment at a time: Geology, v. 36, p. 511–512, https://doi.org/10.1130/focus062008.1.

Miller, R.B., Paterson, S.R., and Matzel, J.P., 2009, Plutonism at different crustal levels: Insights from the ~5–40 km (paleodepth) North Cascades crustal section, Washington, *in* Miller, R.B., and Snoke, A.W., eds., Crustal Cross Sections from the Western North American Cordillera and Elsewhere: Implications for Tectonic and Petrologic Processes: Geological Society of America Special Paper 456, p. 1–26, https://doi.org/10.1130/2009.2456(05).

Muñoz, M., Farías, M., Charrier, R., Fanning, C.M., Polvé, M., and Deckart, K., 2013, Isotopic shifts in the Cenozoic Andean arc of central Chile: Records of an evolving basement throughout cordilleran arc mountain building: Geology, v. 41, p. 931–934, https://doi.org/10.1130/G34178.1.

Muñoz-Gómez, M., Payacán, Í., Gutiérrez, F., Farías, M., Charrier, R., and Polvé, M., 2020, Silicic volcanism triggered by increased denudation rates in the Quaternary Andean arc of central Chile between 33°50′–34°30′S: Lithos, v. 354–355, https://doi.org/10.1016/j.lithos.2019.105242.

Nyström, J.O., Vergara, M., Morata, D., Levi, B., Nystro, J.O., Vergara, M., Morata, D., and Levi, B., 2003, Tertiary volcanism during extension in the Andean foothills of central Chile (33°15′–33°45′S): Geological Society of America Bulletin, v. 115, p. 1523–1537, https://doi.org/10.1130/B25099.1.

Paterson, S.R., 2009, Magmatic tubes, pipes, troughs, diapirs, and plumes: Late-stage convective instabilities resulting in compositional diversity and permeable networks in crystal-rich magmas of the Tuolumne batholith, Sierra Nevada, California: Geosphere, v. 5, p. 496–527, https://doi.org/10.1130/GES00214.1.

Paterson, S.R., and Miller, R.B., 1998, Stoped blocks in plutons: Paleo-plumb bobs, viscometers, or chronometers?: Journal of Structural Geology, v. 20, p. 1261–1272, https://doi.org/10.1016/S0191-8141(98)00066-2.

Paterson, S.R., Fowler, T.K., Schmidt, K.L., Yoshinobu, A.S., Yuan, E.S., and Miller, R.B., 1998, Interpreting magmatic fabric patterns in plutons: Lithos, v. 44, no. 1–2, p. 53–82, https://doi.org/10.1016/S0024-4937(98)00022-X.

Paterson, S.R., Žák, J., and Janousek, V., 2008, Growth of complex sheeted zones during recycling of older magmatic units into younger: Sawmill Canyon area, Tuolumne batholith, Sierra Nevada, California: Journal of Volcanology and Geothermal Research, v. 177, p. 457–484, https://doi.org/10.1016/j.jvolgeores.2008.06.024.

Paterson, S.R., Memeti, V., Pignotta, G., Erdmann, S., Zak, J., Chambers, J., and Ianno, A., 2012, Formation and transfer of stoped blocks into magma chambers: The high-temperature interplay between focused porous flow, cracking, channel flow, host-rock anisotropy, and regional deformation: Geosphere, v. 8, p. 443–469, https://doi.org/10.1130/GES00680.1.

Paterson, S.R., Memeti, V., Mundil, R., and Žák, J., 2016, Repeated, multiscale, magmatic erosion and recycling in an upper-crustal pluton: Implications for magma chamber dynamics and magma volume estimates: The American Mineralogist, v. 101, p. 2176–2198, https://doi.org/10.2138/am-2016-5576.

Paton, C., Hellstrom, J., Paul, B., Woodhead, J., and Hergt, J., 2011, Iolite: Freeware for the visualisation and processing of mass spectrometric data: Journal of Analytical Atomic Spectrometry, v. 26, p. 2508–2518, https://doi.org/10.1039/c1ja10172b.

Payacán, I., Gutiérrez, F., Gelman, S.E., Bachmann, O., and Parada, M.Á., 2014, Comparing magnetic and magmatic fabrics to constrain the magma flow record in La Gloria pluton, central Chile: Journal of Structural Geology, v. 69, p. 32–46, https://doi.org/10.1016/j.jsg.2014.09.015.

Petford, N., Cruden, A.R., McCaffrey, K.J.W., and Vigneresse, J.L., 2000, Granite magma formation, transport and emplacement in the Earth's crust: Nature, v. 408, p. 669–673, https://doi.org/10.1038/35047000.

Piquer, J., Skármeta, J., and Cooke, D.R., 2015, Structural evolution of the Rio Blanco–Los Bronces District, Andes of Central Chile: Controls on stratigraphy, magmatism, and mineralization: Economic Geology, v. 110, p. 1995–2023, https://doi.org/10.2113/econgeo.110.8.1995.

Piquer, J., Berry, R.F., Scott, R.J., and Cooke, D.R., 2016, Arc-oblique fault systems: Their role in the Cenozoic structural evolution and metallogenesis of the Andes of central Chile: Journal of Structural Geology, v. 89, p. 101–117, https://doi.org/10.1016/j.jsg.2016.05.008.

Putirka, K.D., Canchola, J., Rash, J., Smith, O., Torrez, G., Paterson, S.R., and Ducea, M.N., 2014, Pluton assembly and the genesis of granitic magmas: Insights from the GIC pluton in cross section, Sierra Nevada Batholith, California: The American Mineralogist, v. 99, p. 1284–1303, https://doi.org/10.2138/am.2014.4564.

Scaillet, B., Holtz, F., and Pichavant, M., 1998, Phase equilibrium constraints on the viscosity of silicic: 1. Volcanic-plutonic comparison: Journal of Geophysical Research: Solid Earth, v. 103, p. 27,257–27,266, https://doi.org/10.1029/98JB02469.

Schaen, A.J., Cottle, J.M., Singer, B.S., Keller, C.B., Garibaldi, N., and Schoene, B., 2017, Complementary crystal accumulation and rhyolite melt segregation in a late Miocene Andean pluton: Geology, v. 45, p. 835–838, https://doi.org/10.1130/G39167.1.

Schaen, A.J., Singer, B.S., Cottle, J.M., Garibaldi, N., Schoene, B., Satkoski, A.M., and Fournelle, J., 2018, Textural and mineralogical record of low-pressure melt extraction and silicic cumulate formation in the late Miocene Risco Bayo–Huemul Plutonic Complex, Southern Andes: Journal of Petrology, v. 59, p. 1991–2016, https://doi.org/10.1093/petrology/egy087.

Sliwinski, J.T., Bachmann, O., Dungan, M.A., Huber, C., Deering, C.D., Lipman, P.W., Martin, L.H.J., and Liebske, C., 2017, Rapid pre-eruptive thermal rejuvenation in a large silicic magma body: The case of the Masonic Park Tuff, Southern Rocky Mountain volcanic field, CO, USA: Contributions to Mineralogy and Petrology, v. 172, 30, https://doi.org/10.1007/s00410-017-1351-3.

Smith, R.L., 1960, Ash flows: Geological Society of America Bulletin, v. 71, p. 795–841, https://doi.org/10.1130/0016-7606(1960)71[795:AF]2.0.CO;2.

Streckeisen, A., 1974, Classification and nomenclature of plutonic rocks recommendations of the IUGS subcommission on the systematics of igneous rocks: Geologische Rundschau, v. 63, p. 773–786, https://doi.org/10.1007/BF01820841.

Tavazzani, L., Peres, S., Sinigoi, S., Demarchi, G., Economos, R.C., and Quick, J.E., 2020, Timescales and mechanisms of crystal-mush rejuvenation and melt extraction recorded in Permian plutonic and volcanic rocks of the Sesia Magmatic System (Southern Alps, Italy): Journal of Petrology, v. 61, https://doi.org/10.1093/petrology/egaa049.

Thiele, R., 1980, Hoja Santiago, Región Metropolitana. Servicio Nacional de Geología y Minería: Carta Geológica de Chile, v. 29.

Vazquez, J.A., and Reid, M.R., 2002, Time scales of magma storage and differentiation of voluminous high-silica rhyolites at Yellowstone caldera, Wyoming: Contributions to Mineralogy and Petrology, v. 144, p. 274–285, https://doi.org/10.1007/s00410-002-0400-7.

Vernon, R.H., and Collins, W.J., 2011, Structural criteria for identifying granitic cumulates: The Journal of Geology, v. 119, p. 127–142, https://doi.org/10.1086/658198.

Vigneresse, J.L., 2006, Granitic batholiths: From pervasive and continuous melting in the lower crust to discontinuous and spaced plutonism in the upper crust: Earth and Environmental Science Transactions of the Royal Society of Edinburgh, v. 97, p. 311–324, https://doi.org/10.1017/S0263593300001474.

Walker, B.A., Jr., Miller, C.F., Claiborne, L.L., Wooden, J.L., and Miller, J.S., 2007, Geology and geochronology of the Spirit

Mountain batholith, southern Nevada: Implications for timescales and physical processes of batholith construction: Journal of Volcanology and Geothermal Research, v. 167, p. 239–262, https://doi.org/10.1016/j.jvolgeores.2006.12.008.

Watson, E.B., Wark, D.A., and Thomas, J.B., 2006, Crystallization thermometers for zircon and rutile: Contributions to Mineralogy and Petrology, v. 151, p. 413–433, https://doi.org/10.1007/s00410-006-0068-5.

Webber, J.R., Klepeis, K.A., Webb, L.E., Cembrano, J., Morata, D., Mora-Klepeis, G., and Arancibia, G., 2015, Deformation and magma transport in a crystallizing plutonic complex, Coastal Batholith, central Chile: Geosphere, v. 11, p. 1401–1426, https://doi.org/10.1130/GES01107.1.

Weinberg, R.F, 2006, Melt segregation structures in granitic plutons: Geology, v. 34, p. 305–308, https://doi.org/10.1130/G22406.1.

Wiebe, R.A., Manon, M.R., Hawkins, D.P., and McDonough, W.F., 2004, Late-stage mafic injection and thermal rejuvenation of the Vinalhaven Granite, Coastal Maine: Journal of Petrology, v. 45, no. 11, p. 2133–2153, https://doi.org/10.1093/petrology/egh050.

Žák, J., Paterson, S.R., Janousek, V., and Kabele, P., 2009, The Mammoth Peak sheeted complex, Tuolumne batholith, Sierra Nevada, California: A record of initial growth or late thermal contraction in a magma chamber?: Contributions to Mineralogy and Petrology, v. 158, p. 447–470, https://doi.org/10.1007/s00410-009-0391-8.